


## Cytotoxicity activity, *in silico* molecular docking, protein- and DNA-binding study of a new Ni(II) Schiff base complex

Niladri Biswas, Sumit Khanra, Arnab Sarkar, Shamee Bhattacharjee, Deba Prasad Mandal, Ankur Chaudhuri, Sibani Chakraborty & Chirantan Roy Choudhury

To cite this article: Niladri Biswas, Sumit Khanra, Arnab Sarkar, Shamee Bhattacharjee, Deba Prasad Mandal, Ankur Chaudhuri, Sibani Chakraborty & Chirantan Roy Choudhury (2018): Cytotoxicity activity, *in silico* molecular docking, protein- and DNA-binding study of a new Ni(II) Schiff base complex, Journal of Coordination Chemistry

To link to this article: <https://doi.org/10.1080/00958972.2018.1492118>

 View supplementary material 

 Accepted author version posted online: 11 Jul 2018.

 Submit your article to this journal 

 View Crossmark data 

## Cytotoxicity activity, *in silico* molecular docking, protein- and DNA-binding study of a new Ni(II) Schiff base complex

NILADRI BISWAS<sup>a</sup>, SUMIT KHANRA<sup>b</sup>, ARNAB SARKAR<sup>c</sup>, SHAMEE BHATTACHARJEE<sup>c</sup>,  
DEBA PRASAD MANDAL<sup>c</sup>, ANKUR CHAUDHURI<sup>d</sup>, SIBANI CHAKRABORTY<sup>d</sup> and  
CHIRANTAN ROY CHOUDHURY<sup>\*a</sup>

<sup>a</sup>Department of Chemistry, West Bengal State University, Barasat, Kolkata-700126, India

<sup>b</sup>Department of Chemistry, Indian Institute of Science Education and Research, Kolkata Mohanpur - 741 246,  
West Bengal, India

<sup>c</sup>Department of Zoology, West Bengal State University, Barasat, Kolkata-700126, India

<sup>d</sup>Department of Microbiology, West Bengal State University, Barasat, Kolkata-700126, India

One new nickel(II) complex, [Ni(L)] (**1**), was synthesized from the Schiff base ligand derived from pyrrole-2-carboxaldehyde and 1,3-diamino-propane. Complex **1** was characterized by elemental analysis, IR, UV-vis and ESI mass spectroscopy, cyclic voltammetry and single-crystal X-ray structure analysis. Crystallographic results show that two Ni(II) monomeric moieties are present with similar structural features but with slightly different bond lengths and bond angles. The geometry around the Ni(II) center is distorted square planar. DNA-binding properties of complex **1** were well explored by employing UV-vis and fluorescence spectral methods, cyclic voltammetry and by viscosity measurements. Similarly the protein-binding study was studied by multispectroscopic techniques using both BSA and HSA. The cytotoxicity study of the compound has also been evaluated. Notably, the *in vitro* cytotoxicity of complex **1** on two cancer cell lines (AGS and A549) demonstrates that complex **1** has very good anticancer activity. MTT assay, cell-cycle analysis and annexin-V assay have been performed to know the extent of effect of complex **1** as anticancer agent. Further, *in silico* molecular docking study revealed that the nickel(II) complex fits into the minor groove of duplex DNA by hydrophobic interaction with functional groups of B-DNA.

**Keywords:** Nickel(II) complex; X-ray structure; DNA Binding; Protein binding; Cytotoxicity; *In silico* molecular docking

---

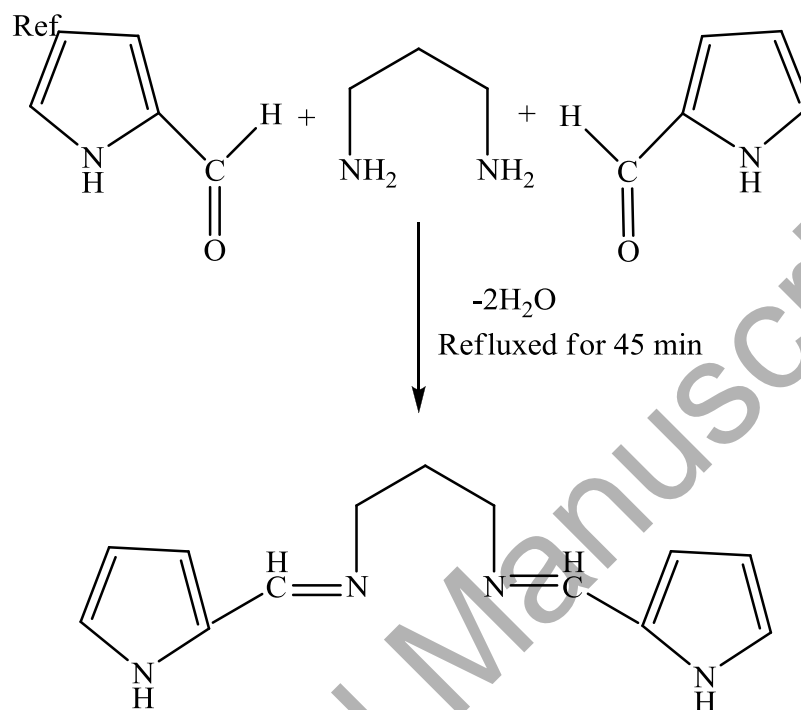
\*Corresponding author. Email: crchoudhury2000@yahoo.com

## 1. Introduction

Nature has already used different transition elements for various biological processes. Based on these ideas, researchers aim at the development of functional models [1-7]. Both the metal ions and ligand parts largely influence the stereochemistry as well as properties of complexes [8]. Nowadays, systematic investigation of anticancer property of metal complexes is one of the main areas of research [8, 9]. But *cis*-platin, which has application in cytotoxic study, is found to have numerous side-effects which ultimately creates the need to develop more effective as well as less toxic anticancer drugs [10, 11]. Recent study focused on the interaction of metal complexes with DNA and understanding the mechanism of action of the probe [12]. Different drugs mostly target DNA and can cause damage of DNA in the target cell [10, 13-15]. In recent time, much research is focused on the development of efficient, target specific, non-toxic drugs [16, 17]. Till now, DNA-targeted nickel complexes are very rare in literature compared to other transition metal complexes like copper, platinum, *etc.* [12, 18-21]. Very few mono- and di-nuclear Ni(II) complexes are available in literature which show very good biological activity [22, 23]. From literature, it is observed that suitable anticancer activity is shown by compounds when aromatic ligands contain N<sub>4</sub> or N<sub>2</sub>O<sub>2</sub> coordination [24-30]. Due to the similarity with HSA, low-cost BSA is mostly used as target protein for interaction study [31-34]. Increased interaction of metal complexes with protein molecules will directly dictate the effective concentration of drugs *in vivo* [10]. So model study of binding of metal complexes *in vitro* can be considered very effective in determining the binding nature of proteins [10, 35].

This fact promoted us to work with Ni(II) metal for the synthesis of metal complexes. The present work reports the synthesis of a Schiff base ligand derived from pyrrole-2-carboxaldehyde and 1,3-diaminopropane (scheme 1) and its nickel(II) complex [Ni(L)] (**1**). The entitled nickel(II)-Schiff base complex is well characterized by IR and UV-vis spectroscopy, cyclic voltammetry and single-crystal X-ray structure analysis. Interaction of complex **1** with CT-DNA was examined by using UV-vis and fluorescence spectral methods, viscosity measurement and cyclic voltammetric study. The protein (BSA and HSA) binding studies were determined with the help of UV-vis as well as fluorescence spectral methods. Theoretical molecular docking studies were also carried out to ascertain the interaction pattern of nickel(II) complex with B-DNA. The cytotoxicity profiles of the titled nickel(II) complex along with cell line study have also been investigated. The significant groove binding of complex **1** with DNA

was explained on the basis of its low intrinsic binding constant value and this groove binding pattern was further explained with the help of viscosity measurements and theoretical molecular docking studies.



Scheme 1. Formation of ligand H<sub>2</sub>L.

## 2. Experimental

### 2.1. Materials

All the required chemicals were of reagent grade and used without purification. Nickel(II) nitrate was purchased from E-Merck and used as received. Pyrrole-2-carboxaldehyde, HSA, BSA and TBAP were purchased from Sigma-Aldrich. Tris-HCl-buffer (pH 7.2) and CT-DNA were purchased from SRL. 1,3-Diaminopropane and ethidium bromide (EB) were purchased from Spectrochem.

### 2.2. Physical measurements

FT-IR spectra were recorded from 400-4000 cm<sup>-1</sup> for complex **1** in solid KBr pellets by using a Perkin-Elmer SPECTRUM - 2 FT-IR spectrophotometer. The UV-vis spectra of the complex

were recorded using a Perkin-Elmer Lambda-35 UV-Vis spectrophotometer in Tris-HCl buffer medium at 300 K. The fluorescence measurements were carried out with a Perkin-Elmer LS 55 fluorescence spectrophotometer in Tris-HCl-buffer medium. ESI mass spectra were recorded in an Agilent 6520 Q-Tof Spectrometer at room temperature in the  $m/z$  range of 0-1000. Elemental analyses were measured with a Perkin-Elmer 2400 II elemental analyzer. During measurements of emission spectra, an excitation and emission slit width of 10 nm was used. All the electrochemical experiments were carried out with three electrode configuration using a CH 660E cyclic voltammeter in Tris-HCl buffer medium. Saturated calomel electrode (SCE) as reference, Pt wire-electrode as counter electrode and glassy carbon electrode as a working electrode were used as three electrode system with tetrabutylammonium perchlorate (TBAP) as a supporting electrolyte at a scan rate of  $50 \text{ mV sec}^{-1}$ . All the electrochemical data were recorded under a dry nitrogen environment. Nitrogen gas was passed into the sample solution at a constant rate for 1 min. The viscosity measurements were carried out using a semi-micro viscometer at  $25 \text{ }^\circ\text{C}$ .

The doubly-distilled water was used to prepare Tris-HCl-buffer maintaining the pH around 7.2. The concentration of CT-DNA in base pairs was calculated with the help of molar extinction coefficient of  $6600 \text{ M}^{-1}\text{cm}^{-1}$  at 260 nm. The ratio of absorbance at 260 and 280 nm was greater than 1.8 which is the indication of high purity of CT-DNA [24].

### **2.3. Synthesis and characterization of ligand and complex**

The tetradentate Schiff base ligand ( $\text{H}_2\text{L}$ ) and complex **1** were prepared according to the following methods. Chemical structure of **1** is shown in figure 1.

### **2.4. Synthesis of tetradentate Schiff base ligand ( $\text{H}_2\text{L}$ )**

Schiff base ( $\text{H}_2\text{L}$ ) was prepared by mixing equimolar concentration of pyrrole-2-carxaldehyde (0.4755 g, 5 mmol) and 1,3-diaminopropane (0.418 mL, 5 mmol) in 50 mL methanolic solution. It was refluxed for 45 min until the color of the solution changed from colorless to straw yellow. The resultant solution was cooled at room temperature during complex preparation.

## 2.5. Synthesis of $[C_{13}H_{14}N_4Ni]$ (**1**)

A methanolic solution of Schiff base ligand (1 mmol) was added to a methanolic solution of  $Ni(NO_3)_2 \cdot 6H_2O$  (0.2908 g, 1 mmol, 10 mL). After mixing, the solution became light red. Then the resultant solution was stirred over a magnetic stirrer for 10 min until the color turned into deep red and it was left for crystallization. After seven days red-colored single-crystals were appeared which were collected by filtration. Yield: 64% (0.254 g). Anal. Calc. for  $[C_{13}H_{14}N_4Ni]$ : C, 57.74; H, 4.91; N, 19.65%. Found: C, 57.71; H, 4.86; N, 19.60%. IR (KBr,  $cm^{-1}$ ): 3467(b), 1595(s), 1275-1436(w) and 489(m).

## 2.6. Single-crystal X-ray diffraction study

Good quality single-crystal of **1** was mounted on a Bruker APEX-II CCD diffractometer, equipped with graphite monochromated Mo  $K\alpha$  radiation ( $\lambda = 0.71073 \text{ \AA}$ ) fine-focus sealed tubes. Intensity data were collected at 292(2) using  $\omega/2\theta$  scans. Crystal data were collected using an APEX2 (Bruker, 2008). Data refinement and reduction were performed using SAINT (Bruker, 2008) software [36]. Multiscan absorption corrections were applied empirically to the intensity values ( $T_{min} = 0.939$  and  $T_{max} = 0.992$ ) using SADABS [36]. The structures were solved by direct methods using the program SIR97 [37] for **1** and refined with full-matrix least-squares based on  $F^2$  using SHELXL-97 [38]. All non-hydrogen atoms were refined anisotropically. C-bound hydrogen atoms were placed geometrically and refined using a riding model approximation. The molecular graphics and crystallographic illustration for **1** was prepared using DIAMOND [39] and ORTEP [40].

## 2.7. DNA-binding experiment

**2.7.1. Electronic absorption spectrophotometric study.** The interaction of complex **1** with CT-DNA was measured in Tris-HCl-buffer solution having pH 7.2. The bulk solution of CT-DNA was prepared by adding CT-DNA in Tris-HCl-buffer solution followed by dilution at 4 °C and it was kept for at least four days. The CT-DNA concentration was measured by its absorption intensity with the help of molar extinction coefficient ( $6600 \text{ M}^{-1} \text{ cm}^{-1}$ ) at 260 nm. A ratio of absorption intensity at 260 and 280 nm of about 1.80:1 signifies that the CT-DNA was sufficiently free from protein molecule and also indicates its purity [41a-b]. The intrinsic binding constant ( $K_b$ ) and binding mode of complex **1** with CT-DNA was determined by the

spectrophotometric titration of fixed metal complex solution (50  $\mu\text{M}$ ) with the continuous variation of CT-DNA solution (0-90  $\mu\text{M}$ ).

**2.7.2. Competitive binding fluorescence measurement.** The interaction between complex **1** and CT-DNA with EB was further investigated by fluorescence study. The solution of EB was prepared by dissolving it into Tris-HCl buffer solution (pH 7.2). Generally the emission intensity of classical intercalator EB increases due to complex formation with CT-DNA [42, 43]. The solution of complex **1** in Tris-HCl buffer was added into the aliquot of CT-DNA pretreated with EB. Significant changes of emission intensities at 607 nm (excitation wavelength 508 nm) were observed. The competitive binding experiment results with the displacement of EB from prepared DNA-EB mixture which results in significant quenching of fluorescence intensity.

**2.7.3. Electrochemical study.** To determine the redox behavior of complex **1**, cyclic voltammetric measurements were performed. This experiment was carried out in a single-compartmental cell at room temperature in Tris-HCl buffer medium using 0.1 M TBAP as supporting electrolyte. A three electrode system containing calomel, Pt-wire and Pt-working as reference, counter and working electrode, respectively, were used for this measurement. Electrochemical experiments in the absence and presence of CT-DNA were carried out to confirm the binding mode of complex **1** with CT-DNA under dry nitrogen atmosphere.

**2.7.4. Viscosity study.** Viscosity measurement was carried out using a semi-micro viscometer suspended vertically in a thermostatic water bath at 25  $^{\circ}\text{C}$ . This experiment was done by keeping CT-DNA concentration fixed (10  $\mu\text{M}$ ) and varying metal complex concentration (10-60  $\mu\text{M}$ ). The average flow times were recorded for three times for each sample with the help of a digital stop watch. The obtained data was plotted as  $(\eta/\eta_0)^{1/3}$  versus  $[\text{complex}]/[\text{DN}]$ , where  $\eta$  and  $\eta_0$  are the viscosity of DNA in the presence and absence of complex **1**, respectively, in the Tris-HCl buffer solution [12].

## **2.8. Protein-binding study**

The binding nature of complex **1** with bovine serum albumin (BSA) and human serum albumin (HSA) were determined by analyzing absorbance as well as fluorescence spectral studies.

Fluorescence spectra were recorded in the range of 280-460 nm (excitation wavelength 279 nm) for both BSA and HSA. The protein stock solutions were prepared by dissolving BSA and HSA into 50 mM Tris-HCl buffer and kept under dark conditions at 4 °C. The protein binding studies were performed by maintaining the fixed concentration of protein solution (40 µM) in Tris-HCl buffer having pH 7.2 and varying the concentration of the Ni(II) complex from 0-60 µM. UV-vis spectral titrations were carried out with concentration of proteins (40 µM) and Ni(II) complex stock solutions (0-70 µM) at room temperature.

### **2.9. Molecular modeling and docking studies**

*In silico* binding mode analysis between synthesized nickel complex and duplex DNA was examined. The crystal structure of duplex DNA d(CGCGAATTCGCG)<sub>2</sub> dodecamer (PDB ID: 1BNA) was retrieved from Protein Data Bank (PDB). All the water molecules were removed from the crystal structure. Hydrogen atoms and Momany-Rone partial charges were added to the duplex DNA. Duplex DNA and complex **1** were typed with CHARMM force-field [44, 45] before molecular docking study. Docking calculations were performed using CDOCKER program [46]. Molecular docking poses of complex **1** were ranked according to CDOCKER interaction energy. Finally energy minimization of the docked receptor-complex **1** was performed for further analysis. All procedures were carried out using Discovery Studio 3.5 software [47].

### **2.10. Cytotoxicity study**

Annexin V-assay Kit was purchased from eBioscience. Anti-mouse anti-bodies against PCNA and GAPDH were procured from Santa Cruz (USA), bacitracin, leupeptin, pepstatin A, PMSF, phosphatase inhibitor cocktails. A-Sepharose beads, RNase, NAC and NBT were purchased from Sigma (St. Louis, MO). Nitrocellulose membrane and filter papers were obtained from Pall Corporation, USA.

Human lung (A549) and gastric (AGS) cancer cell lines were obtained from NCCS Pune. Cells were cultured at 37 °C in humidified atmosphere of 5% CO<sub>2</sub>-95% air. Cell culture medium contains DMEM and F12K (Gibco, invitrogen, USA) supplemented with 10% heat inactivated fetal bovine serum (FBS; Invitrogen.) and 1% penicillin G and streptomycin (Life Technologies,



Rockville, MD, USA). The cells, initially seeded at the concentration of  $10^4$  cells/mm<sup>2</sup>, were incubated at 37 °C with humidity saturated controlled atmosphere and 5% CO<sub>2</sub>.

**2.10.1. Hemolytic assay.** Fresh human blood was centrifuged at 4000Xg for 10 min and the cell pellet was washed thrice and re-suspended in 10 mM PBS at pH 7.4 to obtain a final concentration of  $1.6 \times 10^9$  erythrocytes/mL. Equal volumes of erythrocytes were incubated with varying concentrations of capsaicin and eugenol and with shaking at 37 °C for 1 h. Samples were then subjected to centrifugation at 3500Xg for 10 min at 4 °C. RBC lysis was measured at different peptide concentrations by taking absorbance at an OD of 540 nm. Complete hemolysis (100%) was determined using 1% Triton X 100 as a control. Hemolytic activity of the spice active components was calculated in percentage using the following equation:

$$H=100 \times (Op-Ob)/(Om-Ob)$$

where Op is the optical density of given peptide concentration, Ob is the optical density of buffer and Om is the optical density of Triton X 100.

**2.10.2. Cell viability assay on PBMC.** The Trypan Blue dye exclusion test is used to determine the number of viable cells present in a cell suspension. It is based on the principle that live cells possess intact cell membranes that exclude trypan blue, whereas dead cells do not. The effect of complex **1** on the viability of PBMC cells was determined by Trypan blue exclusion test. Cells were treated with varying of these molecules and at definite time point (24 h) the cells that could exclude the Trypan blue dye were counted in haemocytometer as viable cells.

**2.10.3. MTT assay.** This colorimetric assay is based on the activity of mitochondrial succinate dehydrogenase enzyme in live cells to reduce the yellow water soluble substrate MTT into an insoluble, colored formazan product which is measured spectrophotometrically at 595 nm. Since reduction of MTT can only occur in metabolically active cells, the level of activity is a measure of the viability of cells. The cytotoxicity of these synthetic molecules was tested on AGS and A549 cells by MTT-assay. Briefly,  $2 \times 10^4$  cells were seeded in a 96-well microtitre plate and incubated with different concentrations of these synthetic molecules. After 12 h of exposure to these molecules, 10 µL of MTT (5 mg/mL) was added to each well, and the cells were incubated

in the dark at 37 °C for an additional 4 h. Thereafter, the medium was removed, the formazan crystals were dissolved in 100 µL of dissolving solution (10% SDS in isopropanol), and the absorbance measured at 595 nm.

**2.10.4. Cell cycle distribution analysis.** Cell cycle analysis is a method in that employs flow cytometry to distinguish cells in different phases of the cell cycle based on fluorescence intensity of the stained cells at certain wavelength. For the determination of cell cycle phase distribution of nuclear DNA, *in vitro* AGS, A549 cells ( $1 \times 10^6$  cells) were harvested. After making a single cell suspension, cells were fixed with 3% p-formaldehyde, permeabilized with 0.5% Triton X-100, and nuclear DNA was labeled with propidium iodide (PI, 125 µg/mL) after RNase (40 µg/mL) treatment. Cell cycle phase distribution of nuclear DNA determined on FACS Caliber using Cell Quest Software (Becton-Dickinson Histogram display of DNA content (x-axis, PI fluorescence) versus counts (y-axis) has been displayed.

**2.10.5. Annexin V assay.** Apoptosis assays were carried out based on the instruction from the Annexin V Apoptosis Kit (eBioscience). Briefly, PI and Annexin V were added directly to AGS and A549 cells treated with complex 1 (0.5 µg/mL). The mixture was incubated for 15 min at 37 °C. Cells were fixed and then analyzed on FACS VERSE (equipped with 488 nm Argon laser light source; 515 nm band pass filter, FL1-H, and 623 nm band pass filter, FL2-H) (Becton Dickinson). Electronic compensation of the instrument was done to exclude overlapping of the emission spectra. Total 10,000 events were acquired, the cells were properly gated and dual parameter dot plot of FL1-H (x-axis; Fluos-fluorescence) versus FL2-H (y-axis; PI-fluorescence) shown in logarithmic fluorescence intensity.

**2.10.6. Western blot analysis.** Western blot (also called protein immunoblotting, because an antibody is used to specifically detect its antigen) is a widely accepted analytical technique used to detect specific proteins in the given sample. By analyzing location and intensity of the band formed, expression details of the target proteins in the given cells could be obtained. AGS and A549 cell lysates were obtained and equal amounts of protein from each sample were diluted with loading buffer, denatured, and separated by 10% sodium dodecyl sulfate-polyacrylamide gel electrophoresis (SDS-PAGE) followed by protein transfer to nitrocellulose membrane. The

effect of complex **1** on PCNA expression was checked on AGS and A549 cancer cells. The blot was incubated with anti-PCNA antibody, followed by blotting with HRP-conjugated secondary antibody. The blots were then detected by using a chemiluminescent kit from Thermofisher. This analysis was performed two times.

**2.10.7. Statistical analysis.** The experiments were repeated three times and the data were analyzed statistically. Values have been represented as mean  $\pm$  SD. Data were analyzed and Student's t-test was used to evaluate the statistical differences. Statistical significance was considered when  $P < 0.05$ .

### **3. Results and discussion**

#### **3.1. IR spectra**

IR spectrum of complex **1** is shown in figure S1. Complex **1** exhibits a strong band at  $1595\text{ cm}^{-1}$  which can be assigned to the C=N stretching frequency of azomethine group. The band observed at  $489\text{ cm}^{-1}$  can be attributed to M-N stretching frequency, indicating the participation of azomethine nitrogen in the coordination with the metal ion. Moreover a broad band at  $3467\text{ cm}^{-1}$  appeared which is the characteristic stretching of N-H bond [48]. Pyrrole ring in-plane and out-of-plane vibrations are observed in the region  $1275\text{-}1436\text{ cm}^{-1}$ .

#### **3.2. Electronic absorption spectra**

Absorption spectrum of the complex was recorded in Tris-HCl medium in the range 200-800 nm at 300 K and the spectrum is shown in figure S2. A very low intensity band appeared at 521 nm which corresponds to the  $d \rightarrow d$  transition of Ni(II) having square planar stereochemistry [12]. A high-intensity band at 314 nm and a low-intensity band at 272 nm were observed due to intraligand  $\pi \rightarrow \pi^*$  transitions of the coordinated imines of the ligand. Complex **1** shows two low-energy bands at 433 nm and at 389 nm with a shoulder which can be attributed to  $n \rightarrow \pi^*$  transition [49].

#### **3.3. Cyclic voltammetry**

The electrochemical property of mononuclear Ni(II) complex was investigated by cyclic voltammetry at a scan rate of  $50\text{ mV sec}^{-1}$  having potential range between +2.0 to -2.0 V in Tris-

HCl buffer solution containing TBAP as supporting electrolyte. Figure S3 shows two oxidative peaks at potentials +0.77 to +1.30 V in the anodic region and one reductive peak at -0.86 V in the cathodic region. The oxidation peak at +0.77 V (*versus* SCE) is due to the oxidation of Ni(II) to Ni(III) and the other oxidative wave at +1.30 V can be attributed for the Schiff base oxidation. Complex **1** also showed one irreversible reduction peak at -0.86 (*versus* SCE) which is believed to be due to conversion of Ni(II) to Ni(I) [10].

### 3.4. X-ray crystal structure description

An ORTEP diagram of complex **1** with atom numbering scheme is given in figure 1 and packing diagram is shown in figure S4. Crystal data and details of the structure determination for complex **1** are shown in table 1. The asymmetric unit consists of two molecular units, Ni1 and Ni2, which are crystallographically independent but chemically similar, with slightly different bond lengths and bond angles. Each of the two mononuclear units contains Ni(II) as the central atom having square planar geometry. Each Ni(II) atom (Ni1 and Ni2) is coordinated to two N-atoms coming from 2-pyrolle moiety (N1 and N4 for Ni1; N6 and N8 for Ni2) and another two nitrogen atoms from the imine part of the Schiff base (N2 and N3 for Ni1; N5 and N7 for Ni2). Ni-N bond lengths are in the range 1.8854(19)-1.9119(19) Å, which is similar to the compounds found in the literature [50-53].

The distortion in the Ni coordination environment is clearly shown by the deviations in the *cisoid* and *transoid* N-Ni-N bond angles from their ideal values (table 2). These variations of bond lengths and bond angles clearly indicate the Ni centers (Ni1 and Ni2) are slightly distorted from ideal square planar geometry [52-54].

### 3.5. DNA-binding experiments

**3.5.1. Electronic absorption titration.** Before addition of CT-DNA to complex **1**, its behavior in the Tris-buffer solution (pH ~7.2) at room temperature was observed by UV-vis spectroscopy for 24 h. No dissociation of the ligand (both H<sub>2</sub>L) was observed under these conditions. The UV-vis spectra of complex **1** in DMSO, Tris-buffer medium and acetonitrile are also compared in figure S5 (Supplementary Information). No significant differences were observed in the three spectra showed (refer to table T1 of Supplementary Information). All these data indicate that

complex **1** was stable under the conditions examined (for a detailed discussion about the integrity of complex **1** in aqueous medium, see figure S5).

The most important evidence of the integrity of complex **1** was obtained by ESI mass spectra in positive mode in aqueous medium. The molecular ion peak appeared at  $m/z$  286, which could be attributed to the molecular ion [Ni(L)] peak with ~100% abundance (figure 2). This proved that complex **1** did not undergo any kind of dissociation in aqueous medium under ordinary conditions.

Electronic spectral study is a kind of reliable measurement which is commonly used for investigation about the binding mode of metal complexes with DNA. Due to the cellular receptor property of DNA, the metal complex-DNA interaction is one of the versatile areas of modern research. Generally, metal complexes interact with DNA resulting in either hyperchromism or hypochromism [55a-b]. Usually, during intercalative binding mode, a significant stacking interaction occurs between DNA base pairs and planar aromatic ring of the investigating complex. On the other hand, a prominent increase in absorption of the metal complex with the addition of CT-DNA solution is an effective area of non-intercalative binding. In the case of non-intercalative binding, a reasonable damage of CT-DNA double helix is observed. On the other hand, during groove binding, the metal complex interacts with the external surface of DNA either by van der Waals forces or hydrogen bonding [56a-b]. In the present study, complex **1** displayed two absorption bands in the range of 272-314 nm due to  $\pi \rightarrow \pi^*$  transition and a band at 389 nm with a shoulder due to  $n \rightarrow \pi^*$  transition (figure 3). To determine the binding nature of complex **1** with CT-DNA, fixed concentration of metal complex solution (50  $\mu\text{M}$ ) was titrated with the incremental increase of CT-DNA solution (0-90  $\mu\text{M}$ ). Before obtaining the spectral data, the mixed solution of metal complex and CT-DNA in Tris-HCl-buffer was allowed to equilibrate for 10 min for each titration. After successive addition of CT-DNA to the fixed concentration of metal complex, the  $\pi \rightarrow \pi^*$  transition energy increases along with hyperchromism with slow blue-shift and also a steady decrease in  $n \rightarrow \pi^*$  transition energy. The observed hyperchromism with blue-shift is an indication of hydrogen bonding or van der Waals interaction [57]. So, it is a kind of interaction that has occurred between the external surface of CT-DNA molecule and complex **1** [57-59]. The spectral data of complex **1** in the absence or presence of CT-DNA are shown in figure 3. The binding affinities of the nickel(II) complex with

CT-DNA can be determined by measuring intrinsic binding constant ( $K_b$ ) using equation (1) [60],

$$[\text{DNA}] / [\varepsilon_a - \varepsilon_f] = [\text{DNA}] / [\varepsilon_b - \varepsilon_f] + 1 / K_b [\varepsilon_b - \varepsilon_f] \quad (1)$$

where  $[\text{DNA}]$  is the CT-DNA concentration in base pairs,  $\varepsilon_a$  is the apparent extinction coefficient corresponding to  $A_{\text{obsd}}/[\text{Ni}]$ ,  $\varepsilon_b$  is extinction coefficient of the complex in fully bound form and  $\varepsilon_f$  is extinction coefficient of the complex in unbound form. For complex **1**, when spectral data are fitted in equation (1), we obtained a straight line with a positive slope  $1/([\varepsilon_b - \varepsilon_f])$  and an intercept of  $1/K_b [\varepsilon_b - \varepsilon_f]$ , which are shown in figure 3 (inset). The intrinsic binding constant ( $K_b$ ) for complex **1** can be determined from the ratio of the slope of the Y-intercept [57, 61, 62]. The observed  $K_b$  was  $7.582(\pm 0.016) \times 10^3 \text{ M}^{-1}$ , which is very much lower than that of a classical intercalator such as EB having  $K_b$  value  $1.4 \times 10^5 \text{ M}^{-1}$  [63a]. The observed intrinsic binding constant ( $K_b$ ) of nickel(II) complex is similar to previously reported related Schiff base metal complexes, which are in the range of  $10^3 \text{ M}^{-1}$  [24] to  $10^4 \text{ M}^{-1}$  [63b-h]. This  $K_b$  value confirms that complex **1** moderately bound to CT-DNA by non-intercalative binding mode.

**3.5.2. Competitive binding experiments.** To further investigate the binding mode of complex **1** with CT-DNA, fluorescence spectral titrations were performed. No emission spectrum was found for complex **1** itself or in the presence CT-DNA solution at room temperature. Therefore to determine the binding nature of complex **1**, a competitive binding study has been performed using EB. EB is a well-known planar organic cationic dye whose fluorescence intensity is low but its emission intensity can be enhanced by intercalating into the base pairs of CT-DNA [64, 65]. Therefore, EB is identified as a typical standard of intercalation [66, 67]. Fluorescence binding experiments were carried out for complex **1** (0-50  $\mu\text{M}$ ) in the presence of CT-DNA bound EB in Tris-HCl buffer medium. At 607 nm (figure 4) prominent decrease in the emission intensity of EB-DNA [68, 69] has been observed due to the displacement of EB from CT-DNA–EB mixture. This can be explained due to the fact that the number of binding sites on the CT-DNA was reduced for EB. The EB-displacement study is explained on the basis of Stern-Volmer equation [16],

$$I_0/I = 1 + K_{sv} [Q] \quad (2)$$

where  $I_0$  and  $I$  are the emission intensities in the absence and presence of the quencher, respectively,  $K_{sv}$  is the linear Stern-Volmer quenching constant, and  $[Q]$  is the quencher concentration. From the plot of  $I_0/I$  versus  $[Q]$  is shown in figure 4 (inset). The calculated  $K_{sv}$  value is  $3.534(\pm 0.078) \times 10^4 \text{ M}^{-1}$ . The quenching rate constant ( $K_q$ ) can be determined with the help of the equation  $K_{sv} = K_q \times \tau_0$ , where  $\tau_0$  is the lifetime of fluorophore in the absence of quencher molecule (CT-DNA). Since the fluorescence lifetime is in the order of  $10^{-8}$  s and using this value, quenching rate constant ( $K_q$ ) of complex **1** is  $3.534(\pm 0.078) \times 10^{12} \text{ M}^{-1} \text{ s}^{-1}$ . The observed  $K_q$  value of complex **1** is higher than the limiting diffusion rate constant for a biomacromolecule ( $2.0 \times 10^{10} \text{ M}^{-1} \text{ s}^{-1}$ ) [24]. The above observation illustrates that there is static quenching phenomenon between the fluorophore and the quencher molecule and they form complex in the ground state [24, 70]. The apparent binding constant ( $K_{app}$ ) can be estimated using equation (3),

$$K_{EB} [EB] = K_{app} [\text{complex}] \quad (3)$$

where  $K_{EB} = 1.0 \times 10^5 \text{ M}^{-1}$  which is DNA binding constant of EB,  $[EB]$  is the concentration of EB and  $[\text{complex}]$  is the concentration of the quencher used to determine 50% decrease in the emission intensity of CT-DNA pretreated with EB [71, 72]. The apparent binding constant of complex **1** is  $2.86 \times 10^4 \text{ M}^{-1}$ . Therefore, analyzing the difference in the  $K_{app}$  value of complex **1** to the  $K_{EB}$  value of EB it is clear that complex **1** is not a good classical intercalator like EB [57]. The number of binding sites ( $n$ ) were also determined using Scatchard equation [1, 73],

$$\log [(I_0 - I)/I] = \log K_b + n \log [Q] \quad (4)$$

where  $n$  is the number of binding sites. A straight line was obtained by plotting  $\log [(I_0 - I)/I]$  versus  $\log [Q]$  and from the slope of the plot (figure S6, table 3); the number of binding sites was obtained as  $1.09079 \pm 0.1488$  (table 3).

**3.5.3. Electrochemical study.** Cyclic voltammetry can be regarded as a very sensitive analytical method for the determination about the change of the redox property of metal complex under investigation [24, 74, 75]. Complex **1** displayed two oxidative responses at 0.77 and 1.30 V (vs SCE) and one reductive response at -0.86 V (vs SCE) at a scan rate of  $50 \text{ mV sec}^{-1}$  in Tris-HCl buffer medium containing 0.1 M TBAP as supporting electrolyte. After incremental

addition of CT-DNA solution, the oxidative response at 0.77 V was shifted to 0.63 V (more negative potential value) and the reductive response was also shifted to -0.79 V (more positive potential value). Further addition of CT-DNA solution results in the disappearance of the oxidative response at 0.77 V (figure S7). The observed changes in both anodic and cathodic responses clearly indicate that complex **1** binds with CT-DNA [24, 76]. So, finally it can be assumed that there is a kind of interaction between complex **1** and CT-DNA through which the electron cloud of complex **1** could be “pulled” towards the CT-DNA strands [77].

**3.5.4. Viscosity properties.** Viscosity measurements are a very useful technique to investigate the binding modes between intercalating molecules and DNA. Generally, in classical intercalative binding modes, prominent increase in DNA viscosity is generally observed due to the increase of the length of DNA double helix and also because of accommodation of molecules into the base pairs [78]. On the other hand, in the case of groove binding, DNA viscosity is little influenced by small molecules [79] due to bending or kinking of DNA double helix, which results in reduced effective length of DNA [68, 80]. The effect of complex **1** on CT-DNA viscosity is shown in figure S8. In this figure, it is clear that CT-DNA viscosity in Tris-HCl buffer medium does not show any significant changes with the successive addition of increasing concentration of complex **1**. From this, it is confirmed that the Ni(II) complex does not intercalate into the base pair of CT-DNA double helix. So, the kind of interaction that occurs between complex **1** and the external surface of CT-DNA is either by van der Waals forces or by hydrophobic interaction.

### **3.6. Protein binding studies**

**3.6.1. Electronic absorption titration.** Electronic absorption measurement is a useful method to determine the structural changes and mechanism of complex formation in donor-acceptor systems. To investigate the protein-metal complex molecule relationship, BSA as well as HSA are widely used for this purpose due to their similar structural environment [42, 81-83]. Serum albumin plays an important role in the transport of drugs and metal ions throughout the blood circulatory system. Generally based on the mechanism, quenching process is classified in two categories, one is static and another is dynamic quenching. In the case of static quenching, fluorophore-quencher complex formation occurs in ground state and for dynamic quenching,



quencher molecule and fluorophore come into contact during the short-lived excited state [84]. To confirm whether the titled nickel(II) complex acts as either static or dynamic quencher, UV-vis absorption measurements were carried out. The changes in absorption spectra of both BSA and HSA after successive addition of complex **1** are shown in figures S9A and S9B, respectively. From figure S9, it is clear that the absorption bands of both BSA and HSA increased after the addition of complex **1**. There is a significant change of the absorption band of both the fluorophore molecules BSA and HSA which indicates static quenching process, whereas in dynamic quenching, the absorption spectra of fluorophore molecule is not changed. So, there is a ground-state complex formation between the nickel complex and BSA as well as HSA [81, 84].

**3.6.2. Fluorescence quenching study.** Fluorescence quenching measurements are widely studied for further confirmation regarding the quenching pattern of metal complexes with protein molecules like BSA and HSA [12, 85-87]. Basically protein fluorescence is responsible for three residues of protein, *i.e.* tryptophan, tyrosine and phenylalanine [8]. Binding with these protein molecules can result in either loss or enhancement of the biological properties of the drug molecule. Fluorescence quenching is a phenomenon which reduces the fluorescence intensity of a fluorophore molecule because of the variety of processes involved [88]. In our current study, both BSA and HSA were selected as target protein molecules. In figures 5 and S10, there is a prominent decrease in emission intensity of BSA and HSA at 345 and 341 nm, respectively, after incremental addition of complex **1**. This is due to formation of complex-protein system and alteration of the local environment around tryptophan residue. A significant red-shift was observed for both proteins which indicates a conformational change of tertiary structure of protein molecules. The above quenching effect was analyzed with the help of the Stern-Volmer equation [22, 70],

$$F_0/F = 1 + K_{sv} [Q] \quad (5)$$

where  $F_0$  and  $F$  are the fluorescence intensity in the absence and presence of quencher molecule, respectively.  $K_{sv}$  denotes linear Stern-Volmer quenching constant and  $[Q]$  is the quencher concentration. A plot of  $F_0/F$  versus  $[Q]$  for both BSA and HSA results in a linear plot (insets in figures 5 and S10). The value of  $K_{sv}$  is  $4.83(\pm 0.034) \times 10^4$  and  $3.59(\pm 0.066) \times 10^4 \text{ M}^{-1}$  for BSA and

HSA, respectively. The quenching rate constant ( $K_q$ ) of complex **1** can be obtained using the equation  $K_{sv} = K_q\tau_0$ , where  $\tau_0$  is the average lifetime of protein molecule in the absence of quencher. The  $\tau_0$  value for tryptophan fluorescence in proteins is  $10^{-8}$  s [55, 89]. Complex **1** shows higher quenching rate constant values (for both BSA and HSA) than that of biopolymers ( $2.0 \times 10^{10} \text{ M}^{-1} \text{ s}^{-1}$ ) [89]. The quenching rate constant values of nickel(II) complex with both BSA and HSA are given in table 4. The quenching rate constant ( $K_q$ ) of complex **1** determined by protein quenching procedure is 100 times higher than scatter procedure. The above observation is an indication of static quenching mechanism [90, 91]. Moreover for dynamic quenching, the quenching rate constant ( $K_q$ ) value is normally in the range of  $10^{10} \text{ M}^{-1} \text{ s}^{-1}$  [1]. This behavior is the indication of static interaction between BSA or HSA with complex **1**. When the nickel(II) complex binds to the active site of the protein molecules, the binding constant ( $K_b$ ) as well as number of binding sites ( $n$ ) can be determined using the Scatchard equation [84],

$$\log [(F_0-F)/F] = \log K_b + n \log [Q] \quad (6)$$

By plotting of  $\log [(F_0-F)/F]$  versus  $\log [Q]$  for both proteins (figure S11), the number of binding sites ( $n$ ) and the binding constant ( $K_b$ ) values were determined from the slope and intercept of the plot, respectively. The quenching constant ( $K_q$ ), binding constant ( $K_b$ ) and number of binding site ( $n$ ) values are shown in table 4. By comparing all the experimental data of both BSA and HSA, it is clear that  $K_b$ ,  $K_q$  and  $n$  values of BSA are slightly higher than those of HSA. So, finally it can be concluded that complex **1** binds more strongly to BSA than HSA and so more strongly quenches the emission intensity of BSA than HSA.

### **3.7. Molecular docking of complex 1 with DNA**

In order to gain better insight into the nature of DNA-complex binding, molecular docking study of nickel complex with DNA duplex of sequence  $d(\text{CGCGAATTCGCG})_2$  was performed. Docked complex conformation was examined in terms of interaction energy and hydrophobic interaction between synthesized nickel complex and duplex DNA. *In silico* molecular docking study revealed that the nickel complex fits into the minor groove of duplex DNA by hydrophobic interaction with functional groups of B-DNA (figure 6). From the interaction energy analysis, it

is clear that van der Waals interactions play a predominant role relative to electrostatic interactions in the binding process (table 5).

### **3.8. Cytotoxic profile study**

**3.8.1. Cytotoxicity of complex 1 in normal cells.** Percentage haemolytic activity of complex **1** on human red blood cells is shown in figure S12. Data from hemolytic assay reveals that complex **1** does not show significant haemolysis up to a concentration of 10  $\mu\text{g/mL}$ . Percentage of haemolysis increases quite significantly beyond 10  $\mu\text{g/mL}$ . However, the cytotoxic activity of the compound was found to increase considerably in nucleated cells as determined by Trypan blue exclusion method in human PBMC. Percentage PBMC viability measured by Trypan Blue exclusion method of complex **1** is shown in figure 7. Results suggest that there was significant loss in cell viability beyond a concentration of 0.5  $\mu\text{g/mL}$ .

Haemolytic assay has been done to test the haemolytic effect (lysis of RBC) of the particular compound on human erythrocytes [92] whereas cytotoxicity test on PBMC indicates compound toxicity towards normal cell [93].

Several reports suggest that many drugs have toxic effects on red-blood cell membrane and causes haemolytic anaemia [92, 94]. Therefore, haemolytic assay is needed for a particular drug before use. In our experiment, we have found that compound **1** shows its lytic effect significantly from 10-15  $\mu\text{g/mL}$ .

Peripheral blood mononuclear cell (PBMC) is considered as a normal cell for studying cytotoxic effects of a drug. Several reports indicate that a killing dose of anticancer drug sometimes shows more toxicity to normal cells than cancer cells. So it is necessary to select particular drug concentration that would not kill normal cell but has cytotoxic effects (killing not lysis as in haemolysis) on cancer cell. Our experimental result shows that at 0.5  $\mu\text{g/mL}$  (1/20 of the haemolytic dose), compound **1** shows more killing effect on cancer cells (A549, AGS) than normal cell (PBMC).

**3.8.2. Determination of  $\text{IC}_{50}$  in cancer cell lines by MTT assay.** A549 and AGS cell viability measured by MTT assay at various concentration of complex **1** is shown in figure 8. MTT assay revealed the cytotoxicity of complex **1** in A549 and AGS cells in a concentration-dependent

manner. More than 50% killing was observed at and above a concentration of 0.5  $\mu\text{g}/\text{mL}$  in both cell lines.

As mentioned above, 0.5  $\mu\text{g}/\text{mL}$  is comparatively less toxic to normal cells and is able to induce more than 50% killing in cancer cells. For this reason we have selected 0.5  $\mu\text{g}/\text{mL}$  concentration for further studies on cancer cells.

Coordination of metal ions with ligands is the key-step for cytotoxicity of novel metal complexes [31].  $\text{IC}_{50}$  values of complex **1** against AGS and A549 cell lines are 15.09 and 35.09  $\mu\text{M}$ , respectively. The cytotoxic activity of complex **1** is compared with other similar complexes and shown in table 6 [92-104]. In the cytotoxicity process, coordination of metal ions and the nature of the ring substituents play an important role [31]. The cytotoxic activity of complex **1** is somewhat superior to that of similar complexes reported in the literature (table 6) [92-104]. A valid explanation is the difference in activity against the selected tumor cell lines which can well be explained in terms of variable ligand occupancy with the central metal ion [60]. When ligand:metal is 1:1, then it is a less planar tetrahedral geometry but when the coordination is 2:1, then it must have more planar square planar geometry [60]. In this case, monomeric complex **1** showed higher activity than non-planar complexes (dimer or polymer) (table 6), but are nearly comparable in terms of activity with similar Ni-complexes having planar geometry. Complex **1** has good potential as a cytotoxic agent due to the presence of a pyrrole ring of the coordinated ligand [60]. As not many references available for cytotoxic study with AGS cell line, in this case Ni- and Cu-complexes are cited. Although complex **1** is active against AGS and A549 cell lines under *in vitro* cytotoxicity experiment, the complex is nearly comparable as the effectiveness shown by the standard drug *cis-platin* (table 6).

**3.8.3. Analysis of cell cycle phase distribution of cancer cells.** Figure 9 shows cell-cycle analysis of treated and untreated AGS and A549 cells by flow cytometer using PI as DNA-binding fluorochrome. Treatment with complex **1** resulted in a significant increase in the sub- $\text{G}_0$  region in both AGS and A549 cells (hypoploidy population). As compared to  $4.03 \pm 0.058$  % cells in the hypoploidy region of the AGS control group, complex **1** at 0.5  $\mu\text{g}/\text{mL}$  caused a significant increase in the hypoploidy peak which is  $10.57 \pm 1.08$  %. In the case of A549 cells, hypoploidy population was  $13.7 \pm 1.1$  % in complex **1** treated cells as compared to  $5.3 \pm 0.43$  % in the control

group. Bar diagram representation of cell cycle phase distribution of AGS with wild type and p53 knock out cells is shown in figure S13.

**3.8.4. Effect of complex 1 in AGS and A549 apoptosis.** To confirm the increase in apoptotic induction the complex 1, we performed annexin V/PI assay in all the groups by staining the AGS and A549 cells with FITC tagged annexin V and PI and measuring the fluorescence intensity in a flow cytometer. The results of annexin V assay in AGS and A549 cells are shown in figure 10. The results suggest a significant increase in the percentage of annexin positive cells from  $5.14 \pm 0.04$  % in the AGS control group to  $11.37 \pm 0.59$  % in complex 1 treated groups. Percentage of annexin positive cells increases from  $3.88 \pm 0.04$  % in the A549 control group to  $12.83 \pm 0.89$  % in complex 1 groups.

**3.8.5. Western Blot analysis of protein expressions.** Bar diagram representation of percent Annexin V positive AGS cells from different experimental groups are also given in figure S14. Expression of cell proliferation associated marker, proliferating cell nuclear antigen (PCNA), was found to reduce significantly upon complex 1 treatment in both AGS and A549 cells.

#### 4. Conclusion

One nickel(II) complex with N<sub>4</sub>-chelation [Ni(L)] has been synthesized and characterized by structural, analytical as well as spectroscopic methods. DNA-binding activity of complex 1 was determined using UV-vis absorption, competitive fluorescence titration, cyclic voltammetry and viscosity measurements. The low value (in the order  $10^3 \text{ M}^{-1}$ ) of the binding constant suggests groove mode of binding. This fact was further established by *in silico* molecular docking study. Biological profile of complex 1 as anticancer agent is also studied. Complex 1 has been found to exhibit *in vitro* antiproliferative activity towards two cell lines, AGS and A549 cancer cells. MTT assay, cell-cycle analysis and annexin-V assay have been performed to know the extent of effect of complex 1 as an anticancer agent.

All the results demonstrate that complex 1 has very good anticancer activity.

## Supplementary data

CCDC 1008381 contains the supplementary crystallographic data for complex **1**. These data can be obtained free of charge via <http://www.ccdc.cam.ac.uk/conts/retrieving.html>, or from the Cambridge Crystallographic Data Centre, 12 Union Road, Cambridge CB2 1EZ, UK; Fax: (+44) 1223-336-033; or E-mail: [deposit@ccdc.cam.ac.uk](mailto:deposit@ccdc.cam.ac.uk). Supplementary data associated with this article can be found in the online version.

## Acknowledgement

C. Roy Choudhury acknowledges DST-FIST (Project No. SR/FST/CSI-246/2012) New Delhi, Govt. of India for instrumental support under capital heads.

## Disclosure statement

No potential conflict of interest was reported by the authors.

## References

- [1] M. Das, R. Nasani, M. Saha, S.M. Mobin, S. Mukhopadhyay. *Dalton Trans.*, **44**, 2299 (2015).
- [2] D. Tietze, M. Tischler, S. Voigt, D. Imhof, O. Ohlenschläger, M. Görlach, G. Buntkowsky. *Chem. Eur. J.*, **16**, 7572 (2010).
- [3] S.M. Barnett, K.I. Goldberg, J.M. Mayer. *Nat. Chem.*, **4**, 498 (2012).
- [4] S. Shaik. *Nat. Chem.*, **2**, 347 (2010).
- [5] A. Mukherjee, Biomimetics Learning from Nature, InTech (2010).
- [6] D.M.L.D. Bethany, N. Wigington, T.R. Cundari, D.L. Thorn, S.K. Hanson, S.L. Scott. *Chem.-Eur. J.*, **18**, 14981 (2012).
- [7] B. Meunier, Biomimetic oxidations catalyzed by transition metal complexes, Imperial College Press (2000).
- [8] M. Niu, Z. Li, H. Li, X. Li, J. Dou, S. Wang. *RSC Adv.*, **5**, 37085 (2015).
- [9] (a) M.J. Li, T.Y. Lan, X.H. Cao, H.H. Yang, Y. Shi, C. Yi, G.N. Chen. *Dalton Trans.*, **43**, 2789 (2014). (b) N. Pravin, N. Raman. *Eur. J. Med. Chem.*, **85**, 675 (2014). (c) N.P.E. Barry, P.J. Sadler. *Chem. Commun.*, **49**, 5106 (2013). (d) S.S. Bhat, A.A. Kumbhar, H. Heptullah, A.A. Khan, V.V. Gobre, S.P. Gejji, V.G. Puranik. *Inorg. Chem.*, **50**, 545

- (2011). (e) S. Ramakrishnan, D. Shakthipriya, E. Suresh, V.S. Periasamy, M.A. Akbarsha, M. Palaniandavar. *Inorg. Chem.*, **50**, 6458 (2011). (f) F. Arjmand, F. Sayeed, M. Muddassir. *J. Photochem. Photobiol. B*, **103**, 166 (2011).
- [10] S. Poornima, K. Gunasekaran, M. Kandaswamy. *Dalton Trans.*, **44**, 16361 (2015).
- [11] M.-J. Li, T.-Y. Lan, X.-H. Cao, H.-H. Yang, Y. Shi, C. Yi, G.-N. Chen. *Dalton Trans.*, **43**, 2789 (2014).
- [12] R.R. Kumar, M.K.M. Subarkhan, R. Ramesh. *RSC Adv.*, **5**, 46760 (2015).
- [13] A. Nori, J. Kopecek. *Adv. Drug Delivery Rev.*, **57**, 609 (2005).
- [14] Y. Xie, G.G. Miller, S.A. Cubitt, K.J. Soderlind, M.J. Allalunis-Turner, J.W. Lown. *Anti-Cancer Drug Des.*, **12**, 169 (1997).
- [15] M. Shi, K. Ho, A. Keating, M.S. Shoichet. *Adv. Funct. Mater.*, **19**, 1689 (2009).
- [16] P. Vijayan, P. Viswanathamurthi, K. Velmurugan, R. Nandhakumar, M.D. Balakumaran, P.T. Kalaichelvan, J.G. Malecki. *RSC Adv.*, **5**, 103321 (2015).
- [17] J.C. Venter, M.D. Adams, E.W. Myers, P.W. Li. *Science*, **291**, 1304 (2001).
- [18] S.H. van Rijt, P.J. Sadler. *Drug Discovery Today*, **14**, 1089 (2009).
- [19] H. Mansouri-Torshizi, M. Saeidifar, F. Khosravi, A. Divsalar, A.A. Saboury, F. Hassani. *Bioinorg. Chem. Appl.*, **2011**, 394506 (2011).
- [20] D. Palanimuthu, S.V. Shinde, K. Somasundaram, A.G. Samuelson. *J. Med. Chem.*, **56**, 722 (2013).
- [21] P. Sathyadevi, P. Krishnamoorthy, N.S.P. Bhuvanesh, P. Kalaiselvi, V. Vijaya Padma, N. Dharmaraj. *Eur. J. Med. Chem.*, **55**, 420 (2012).
- [22] S. Mistri, H. Puschmann, S.C. Manna. *Polyhedron*, **115**, 155 (2016).
- [23] (a) Q.X. Yang, L.Z. Gang, L.W. Sheng, Z.H. Liang. *Chin. J. Struct. Chem.*, **27**, 707 (2008). (b) C.S. Liu, H. Zhang, R. Chen, X.S. Shi, X.H. Bu, M. Yang. *Chem. Pharm. Bull.*, **55**, 996 (2007). (c) S. Poornima, K. Gunasekaran, M. Kandaswamy. *Dalton Trans.*, **44**, 16361 (2015).
- [24] Z. Mandegani, Z. Asadi, M. Asadi, H. R. Karbalaeei-Heidari, B. Rastegari. *Dalton Trans.*, **45**, 6592 (2016).
- [25] M.J. Bloemink, J. Reedijk, Metal Ions in Biological Systems, A. Sigel, H. Sigel (Eds.), Marcel Dekker, Inc. New York, **32**, 641 (1996).
- [26] K.E. Erkkila, D.T. Odom, J.K. Barton. *Chem. Rev.*, **99**, 2777 (1999).

- [27] C. Metcalfe, J.A. Thomas. *Chem. Soc. Rev.*, **32**, 215 (2003).
- [28] R.B. Nair, E.S. Teng, S.L. Kirkland, C.J. Murphy. *Inorg. Chem.*, **37**, 139 (1998).
- [29] M. Cusumano, M.L. Di Pietro, A. Giannetto, P.A. Vainiglia. *J. Inorg. Biochem.*, **99**, 560 (2005).
- [30] A. Juris, V. Balzani, F. Barigelletti, S. Campagna, P.L. Belser, A. von Zelewsky. *Coord. Chem. Rev.*, **84**, 85 (1988).
- [31] M. Niu, M. Hong, G. Chang, Xi. Li, Z. Li. *J. Photochem. Photobiol. B*, **148**, 232 (2015).
- [32] X.M. He, D.C. Carter. *Nature*, **358**, 209 (1992).
- [33] P. Ju, H. Fan, T. Liu, L. Cui, S. Ai, X. Wu. *Biol. Trace Elem. Res.*, **144**, 1405 (2011).
- [34] M. Estévez, P. Kylli, E. Puolanne, R. Kivikari, M. Heinonen. *J. Agric. Food Chem.*, **56**, 10933 (2008).
- [35] (a) Q.X. Yang, L.Z. Gang, L.W. Sheng, Z.H. Liang. *Chin. J. Struct. Chem.*, **27**, 707 (2008). (b) C.S. Liu, H. Zhang, R. Chen, X.S. Shi, X. H. Bu, M. Yang. *Chem. Pharm. Bull.*, **55**, 996 (2007).
- [36] Bruker (2000, 2008). SADABS, SMART and SAINT. Bruker AXS Inc., Madison, Wisconsin, USA.
- [37] A. Altomare, M.C. Burla, M. Camalli, G.L. Cascarano, C. Giacovazzo, A. Guagliardi, A.G.G. Moliterni, G. Polidori, R. Spagna. *J. Appl. Cryst.*, **32**, 115 (1999).
- [38] G.M. Sheldrick. *Acta Cryst. A*, **64**, 112 (2008).
- [39] K. Brandenburg, K. Brandenburg, and H. Putz, or K. Brandenburg, and M. Berndt (1999). DIAMOND. Crystal Impact GbR, Bonn, Germany.
- [40] L.J. Farrugia. *J. Appl. Cryst.*, **30**, 565 (1997).
- [41] (a) P. Adak, B. Ghosh, A. Bauza, A. Frontera, A.J. Blake, M. Corbella, C.D. Mukhopadhyay, S.K. Chattopadhyay. *RSC Adv.*, **6**, 86851 (2016). (b) S. Satyanarayana, J.C. Dabrowiak, J.B. Chaires. *Biochemistry*, **32**, 2573 (1993).
- [42] S.A. Ingle, A.N. Kate, A.A. Khumbhar, A.A. Khan, S.S. Rao, S.P. Gejji. *RSC Adv.*, **5**, 47476 (2015).
- [43] J.B. Lepecq, C. Paoletti. *J. Mol. Biol.*, **27**, 87 (1967).
- [44] S.E. Feller, A.D. Mackerell. *J. Phys. Chem. B*, **104**, 7510 (2000).
- [45] A.D. Mackerell, D. Bashford, M. Bellott, R.L. Dunbrack, J.D. Evanseck, M. Karplus. *J. Phys. Chem. B*, **102**, 3586 (1998).



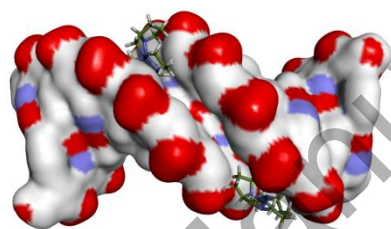
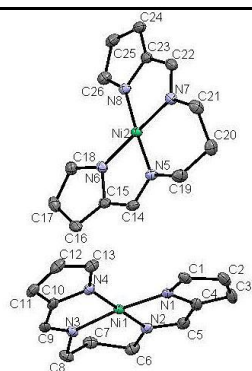
- [46] G. Wu, D.H. Robertson, C.L. Brooks III, M. Vieth. Detailed Analysis of Grid-Based Molecular Docking: A Case Study of CDOCKER - A CHARMM-Based MD Docking Algorithm. *J. Comp. Chem.*, **24**, 1549 (2003).
- [47] Accelrys Discovery Studio Visualiser v 3.5.0.12158, San Diego: Accelrys Software Inc.
- [48] K. Nakamoto, Infrared and Raman Spectra of Inorganic and Coordination Compounds, vol. 23, Wiley, New York (1997).
- [49] A.B.P. Lever, Inorganic Electronic Spectroscopy, 2nd Edn., Elsevier, Amsterdam (1984).
- [50] P.K. Suganthy, R.N. Prabhu, V.S. Sridevi. *Tetrahedron Lett.*, **54**, 5695 (2013).
- [51] R. Buchtik, Z. Travnicek, J. Vanco, R. Harchela, Z. Dvorak. *Dalton Trans.*, **40**, 9404 (2011).
- [52] S.Y. Lee, A. Hille, C. Frias, B. Kater, B. Bonitzki, S. Wolfi, H. Scheffler, A. Prokop, R. Gust. *J. Med. Chem.*, **53**, 6064 (2010).
- [53] S. Mukhopadhyay, D. Mandal, D. Ghosh, I. Goldberg, M. Chaudhury. *Inorg. Chem.*, **42**, 8439 (2003).
- [54] P. Sathyadevi, P. Krishnamoorthy, R.R. Butorac, A.H. Cowly, N.S.P. Bhuvanesh, N. Dharmaraj. *Dalton Trans.*, **40**, 9690 (2011).
- [55] (a) Z. Shokohi-pour, H. Chiniforoshan, A. A. Momtazi-borojeni, B. Notash. *J. Photochem. Photobiol. B*, **162**, 34 (2016). (b) B. Peng, H. Chao, B. Sun, H. Li, F. Gao, L.-N. Ji. *J. Inorg. Biochem.*, **100**, 1487 (2006).
- [56] (a) X. Totta, A.G. Hatzidimitriou, A.N. Papadopoulos, G. Psomas. *Polyhedron*, **117**, 172 (2016). (b) B.M. Zeglis, V.C. Pierre, J.K. Barton. *Chem. Commun.*, 4565 (2007).
- [57] S. Mondal, B. Pakhira, A.J. Blake, M.G.B. Drew, S. K. Chattopadhyay. *Polyhedron*, **117**, 327 (2016).
- [58] S. Sarkar, A. Mondal, D. Chopra, J. Ribas, K. Rajak. *Eur. J. Inorg. Chem.*, 3510 (2006).
- [59] (a) J. Chen, X. Wang, Y. Shao, J. Zhu, Y. Zhu, Y. Li, Q. Xu, Z. Guo. *Inorg. Chem.*, **46**, 3306 (2007). (b) A. Dimitrakopoulou, C. Dendrinou-Samara, A.A. Pantazaki, M. Alexiou, E. Nordlander, D.P. Kessissoglou. *J. Inorg. Biochem.*, **102**, 618 (2008).
- [60] P. Krishnamoorthy, P. Sathyadevi, R.R. Butorac, A.H. Cowley, N.S.P. Bhuvanesh, N. Dharmaraj. *Dalton Trans.*, **41**, 4423 (2012).
- [61] A.M. Pyle, J.P. Rehmman, J.P. Meshoyrer, C.V. Kumar, N.J. Turro, J.K. Barton. *J. Am. Chem. Soc.*, **111**, 3051 (1989).

- [62] A. Wolfe, G.H. Shimer Jr., T. Meehan. *Biochemistry*, **26**, 6392 (1987).
- [63] (a) W.D. Wilson, L. Ratmeyer, M. Zhao, L. Strekowski, D. Boykin. *Biochemistry*, **32**, 4098 (1993). (b) M. Waring. *J. Mol. Biol.*, **13**, 269 (1965). (c) T.-R. Li, Z.-Y. Yang, B.-D. Wang, D.-D. Qin. *Eur. J. Med. Chem.*, **43**, 1688 (2008). (d) A. Tarushi, J. Kljun, I. Turel, A.A. Pantazaki, G. Psomas, D.P. Kessissoglou. *New J. Chem.*, **37**, 342 (2013). (e) A. Tarushi, C.P. Raptopoulou, V. Psycharis, A. Terzis, G. Psomas, D.P. Kessissoglou. *Bioorg. Med. Chem.*, **18**, 2678 (2010). (f) S. Sallam, A. Abba. *J. Lumin.*, **136**, 212 (2013). (g) X.-L. Wang, H. Chao, H. Li, X.-L. Hong, Y.-J. Liu, L.-F. Tan, L.-N. Ji. *J. Inorg. Biochem.*, **98**, 1143 (2004). (h) Q.-L. Zhang, J.-G. Liu, J. Liu, G.-Q. Xue, H. Li, J.-Z. Liu, H. Zhou, L.-H. Qu, L.-N. Ji. *J. Inorg. Biochem.*, **85**, 291 (2001).
- [64] F.J. Meyer-Almes, D. Porschke. *Biochemistry*, **32**, 4246 (1993).
- [65] G.M. Howe, K.C. Wu, W.R. Bauer. *Biochemistry*, **19**, 339 (1976).
- [66] M. Muralisankar, S. Sujith, N.S.P. Bhuvanesh, A. Sreekanth. *Polyhedron*, **118**, 103 (2016).
- [67] K. Jeyalakshmi, Y. Arun, N.S.P. Bhuvanesh, P.T. Perumal, A. Sreekanth, R. Karvembu. *Inorg. Chem. Front.*, **2**, 780 (2015).
- [68] A. Rambabu, M.P. Kumar, S. Tejaswi, N. Vamsikrishna, Shivaraj. *J. Photochem. Photobiol. B*, **165**, 147 (2016).
- [69] B.C. Baguley, M. LeBret. *Biochemistry*, **23**, 937 (1984).
- [70] R. Lakowicz, Principles of fluorescence spectroscopy, Springer Science & Business Media (2013).
- [71] X. Z. Feng, Z. Yang, L.J. Wang, C. Bai. *Talanta*, **47**, 1223 (1998).
- [72] N. Raman, C. Thangaraja. S. Johnsonraja. *Central Eur. J. Chem.*, **3**, 537 (2005).
- [73] P. Li, M. Niu, M. Hong, S. Cheng, J. Dou. *J. Inorg. Biochem.*, **137**, 101 (2014).
- [74] S. Srinivasan, J. Annaraj, P. Athappan. *J. Inorg. Biochem.*, **99**, 876 (2005).
- [75] A.M. Leone, J D. Tibodeau, S.H. Bull, S.W. Feldberg, H.H. Thorp, R.W. Murray. *J. Am. Chem. Soc.*, **125**, 6784 (2003).
- [76] N. Muhammad, A. Shah, S. Shuja, S. Ali, R. Qureshi, A. Meetsma, M.N. Tahir. *J. Organomet. Chem.*, **694**, 3431 (2009).
- [77] S. Banerjee, S. Mondal, S. Sen, S. Das, D.L. Hughes, C. Rizzoli, C. Desplanches, C. Mandal, S. Mitra. *Dalton Trans.*, 6849 (2009).

- [78] J.M. Kelly, A.B. Tossi, D.J. McConnell, C. OhUigin. *Nucleic Acids Res.*, **13**, 6017 (1985).
- [79] S. Satyanarayana, J.C. Dabrowiak, J.B. Chaires. *Biochemistry*, **31**, 9319 (1992).
- [80] F. Arjmand, S. Parveen, M. Afzal, M. Shahi. *J. Photochem. Photobiol. B*, **114**, 15 (2012).
- [81] S. Rajalakshmi, M.S. Kiran, V.G. Vaidyanathan, E.R.A. Singam, V. Subramaniam, B.U. Nair. *Eur. J. Med. Chem.*, **70**, 280 (2013).
- [82] M. Ganeshpandian, R. Loganathan, S. Ramakrishnan, A. Riyasdeen, M.A. Akbarsha, M. Palaniandavar. *Polyhedron*, **52**, 924 (2013).
- [83] D. Senthil Raja, G. Paramaguru, N.S.P. Bhuvanesh, J.H. Reibenspies, R. Renganathan, K. Natarajan. *Dalton Trans.*, **40**, 4548 (2011).
- [84] R. Prabhakaran, P. Kalaivani, P. Poornima, F. Dallemer, G. Paramaguru, V. Vijaya Padma, R. Renganathan, R. Huang, K. Natarajan. *Dalton Trans.*, **41**, 9323 (2012).
- [85] L. Messori, P. Orioli, D. Vullo, E. Alessio, E. Iengo. *Eur. J. Biochem.*, **267**, 1206 (2000).
- [86] Y. Wang, X. Wang, J. Wang, Y. Zhao, W. He, Z. Guo. *Inorg. Chem.*, **50**, 12661 (2011).
- [87] S.-J. Lau, B. Sarkar. *J. Biol. Chem.*, **246**, 5938 (1971).
- [88] P. Sathyadevi, P. Krishnamoorthy, R.R. Butorac, A.H. Cowley, N. Dharmaraj. *Metallomics*, **4**, 498 (2012).
- [89] C.Y. Gao, X. Qiao, Z.Y. Ma, Z.G. Wang, J. Lu, J.L. Tian, J.Y. Xu, S.P. Yan. *Dalton Trans.*, **41**, 12220 (2012).
- [90] H.Y. Liu, Z.H. Xu. *Chem. Pharm. Bull.*, **57**, 1237 (2009).
- [91] P. Kalaivani, R. Prabhakaran, M.V. Kaveri, R. Huang, R.J. Staples, K. Natarajan. *Inorg. Chim. Acta*, **405**, 415 (2013).
- [92] R.A. Sacher, V.M. Priego, M.S. Schanfield, E.M. Bonnem. *Br. J. Haematol.*, **54**, 543, (1983).
- [93] R.C. Rees, A.A. Platts. *J. Immunol. Methods*, **62**, 79 (1983).
- [94] L.D. Petz, G. Garratty. *Clin. Haematol.*, **4**, 181 (1975).
- [95] M.M. Abd-Elzaher, A.A. Labib, H.A. Mousa, S.A. Moustafa, M.M. Ali, A.A. El-Rashedy. *Beni-suff university journal of basic and applied sciences*, **5**, 85 (2016).
- [96] Y. Li, Z. Yang, M. Zhou, Y. Li, J. He, X. Wang, Z. Lin. *RSC Adv.*, **7**, 41527 (2017).
- [97] Z. Li, H. Yan, G. Chang, M. Hong, J. Dou, M. Niu. *J. Photochem. Photobiol. B, Biol.*, **163**, 403 (2016).

- [98] S. Kathiresan, S. Mugesh, J. Annaraj, M. Murugan. *New J. Chem.*, **41**, 1267 (2017).
- [99] N. Biswas, S. Khanra, A. Sarkar, S. Bhattacharjee, D.P. Mandal, A. Chaudhuri, S. Chakraborty, C.R. Choudhury. *New J. Chem.*, **41**, 12996 (2017).
- [100] P. Kalaivani, R. Prabhakaran, F. Dallemer, K. Natarajan. *RSC Adv.*, **4**, 51850 (2014).
- [101] P. Kalaivani, R. Prabhakaran, F. Dallemer, E. Vaishnavi, P. Poornima, V. Vijaya Padma, R. Renganathan, K. Natarajan. *J. Organomet. Chem.*, **762**, 67 (2014).
- [102] G. Kalaiarasi, C. Umadevi, A. Shanmugapriya, P. Kalaivani, F. Dallemer, R. Prabhakaran. *Inorg. Chim. Acta*, **453**, 547 (2016).
- [103] J. Haribabu, K. Jeyalakshmi, Y. Arun, N.S.P. Bhuvanesh, P.T. Perumalm, R. Karvembu. *RSC Adv.*, **5**, 46031 (2015).
- [104] P. Kalaivani, R. Prabhakaran, E. Vaishnavi, T. Rueffer, H. Lang, P. Poornima, R. Renganathan, V. Vijaya Padma, K. Natarajan. *Inorg. Chem. Front.*, **1**, 311 (2014).
- [105] S. Kathiresan, S. Mugesh, M. Murugan, F. Ahamed, J. Annaraj. *RSC Adv.*, **6**, 1810 (2016).
- [106] Y. Li, Z. Yang, M. Zhou, Y. Li. *RSC Adv.*, **7**, 49404 (2017).
- [107] S. Kathiresan, J. Annaraj, N.S.P. Bhuvanesh. *Chem. Select*, **2**, 5475 (2017).

## Graphical abstract



Accepted Manuscript

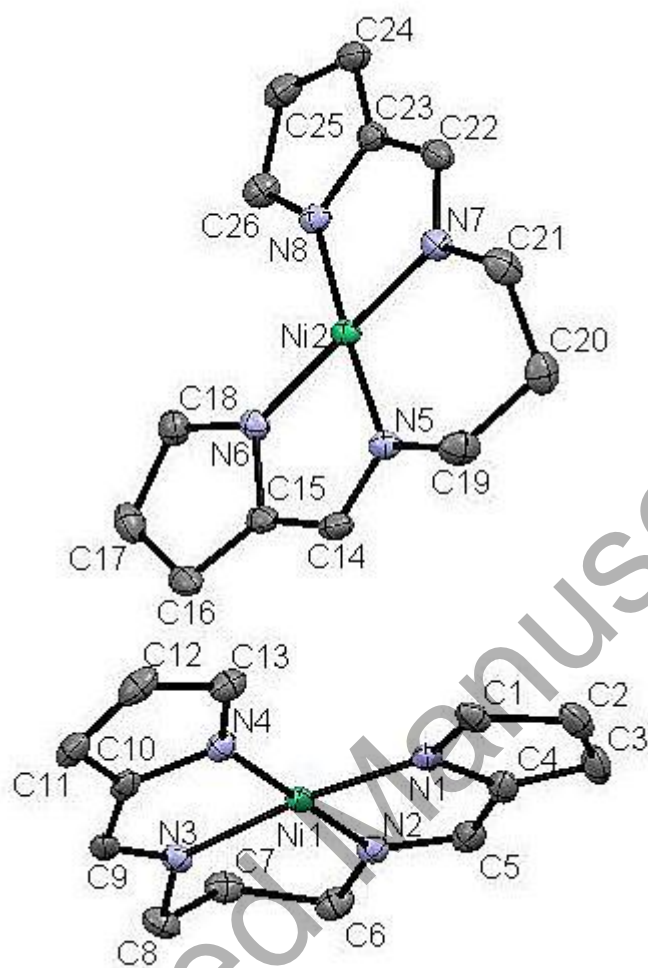


Figure 1. ORTEP view of complex 1 with displacement ellipsoids drawn at 50% probability level (hydrogens are omitted for clarity).

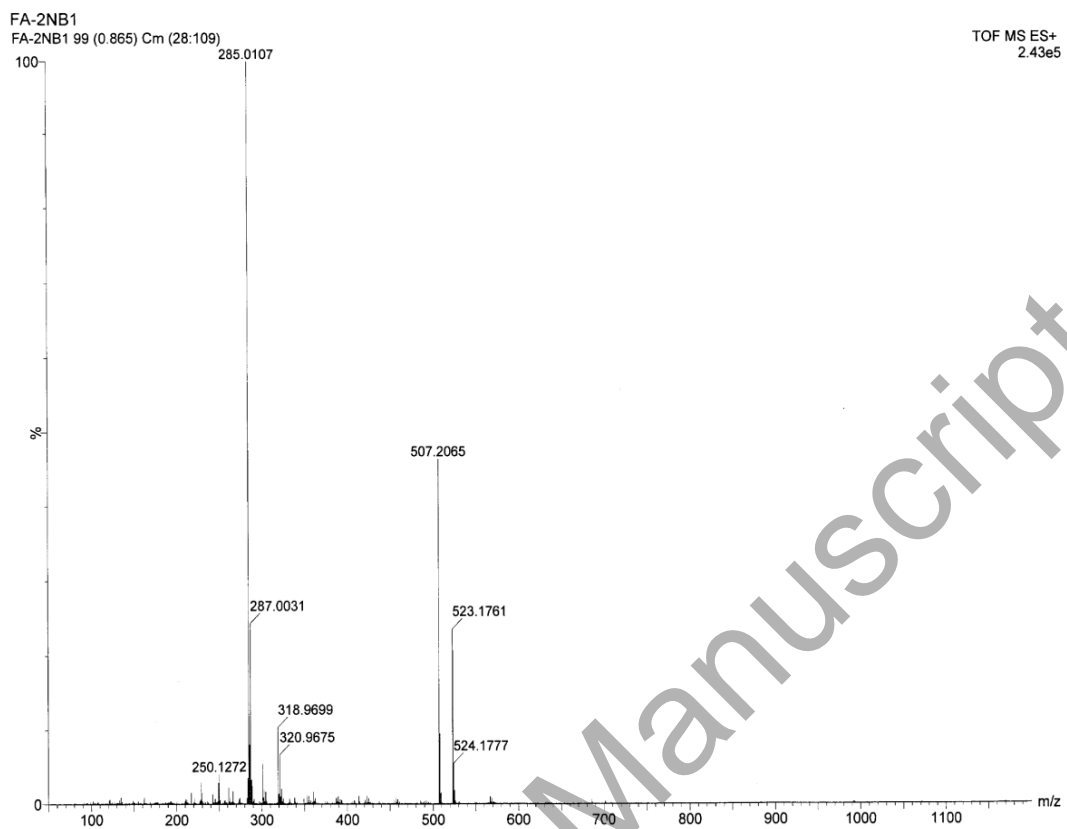


Figure 2. ESI mass spectrum of complex 1.

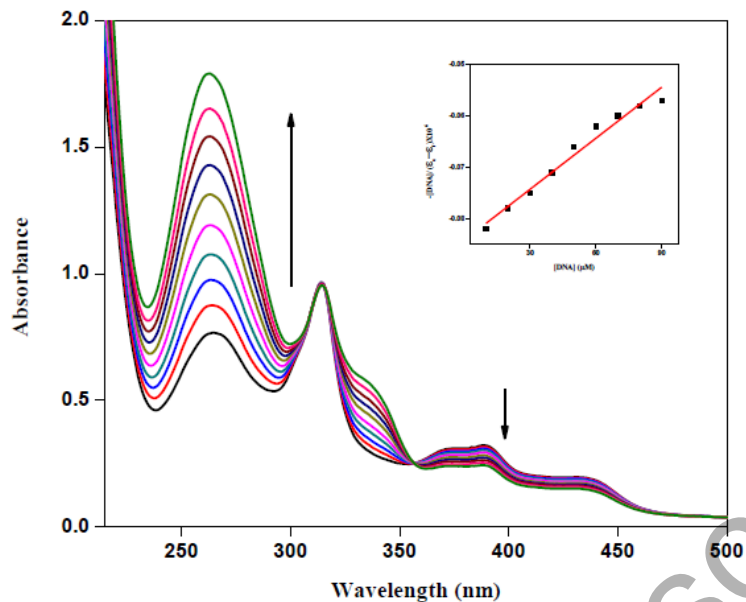


Figure 3. UV-vis absorption spectra of complex **1** in Tris-HCl buffer medium in the presence of CT-DNA. [Complex] = 50  $\mu M$ , [CT-DNA] = 0-90  $\mu M$ . The arrow indicates the absorbance spectral changes on increasing CT-DNA concentration. Inset shows the plot of  $[DNA]/[\epsilon_a - \epsilon_f]$  versus  $[DNA]$  for the calculation of intrinsic binding constant ( $K_b$ ) of complex **1**.



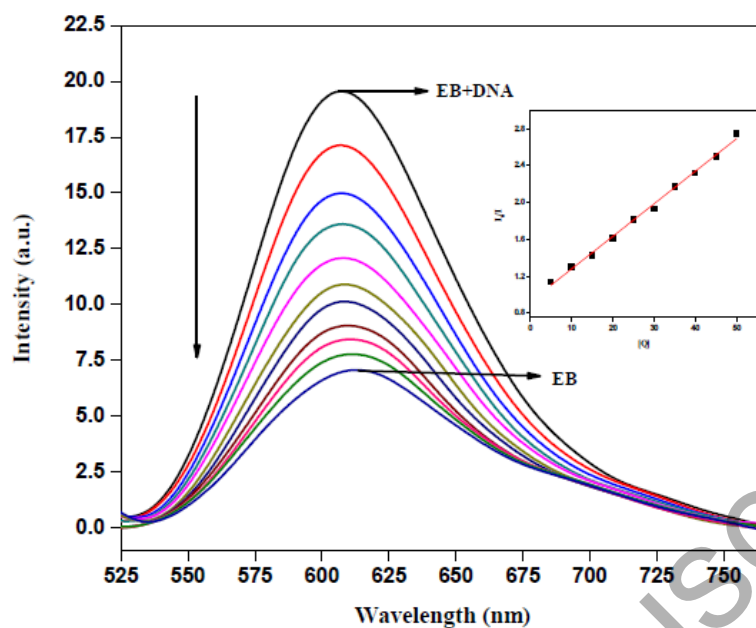


Figure 4. Fluorescence emission spectra of EB bound CT-DNA in the presence of complex **1**. [DNA] = 20  $\mu$ M, [EB] = 10  $\mu$ M and [complex] = 0-50  $\mu$ M. Inset shows plot of  $I_0/I$  versus  $[Q]$  for the determination of quenching constant of complex **1**.

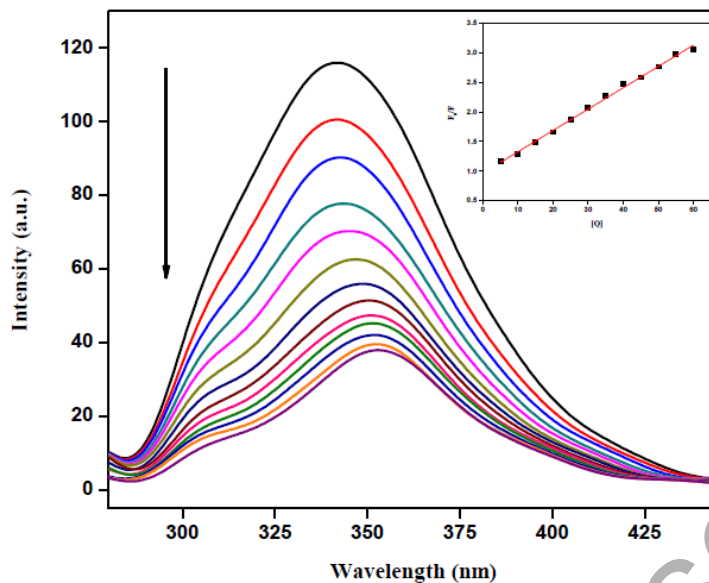


Figure 5. The emission spectra of HSA (40  $\mu\text{M}$ :  $\lambda_{\text{exi}} = 279 \text{ nm}$ ;  $\lambda_{\text{emi}} = 341 \text{ nm}$ ) at various concentrations of complex **1** (0-60  $\mu\text{M}$ ). The arrow indicates decrease in fluorescence intensities upon increasing the concentrations of the nickel complex. The inset shows Stern-Volmer linear plot of  $F_0/F$  versus  $[Q]$  of complex **1** with HSA.

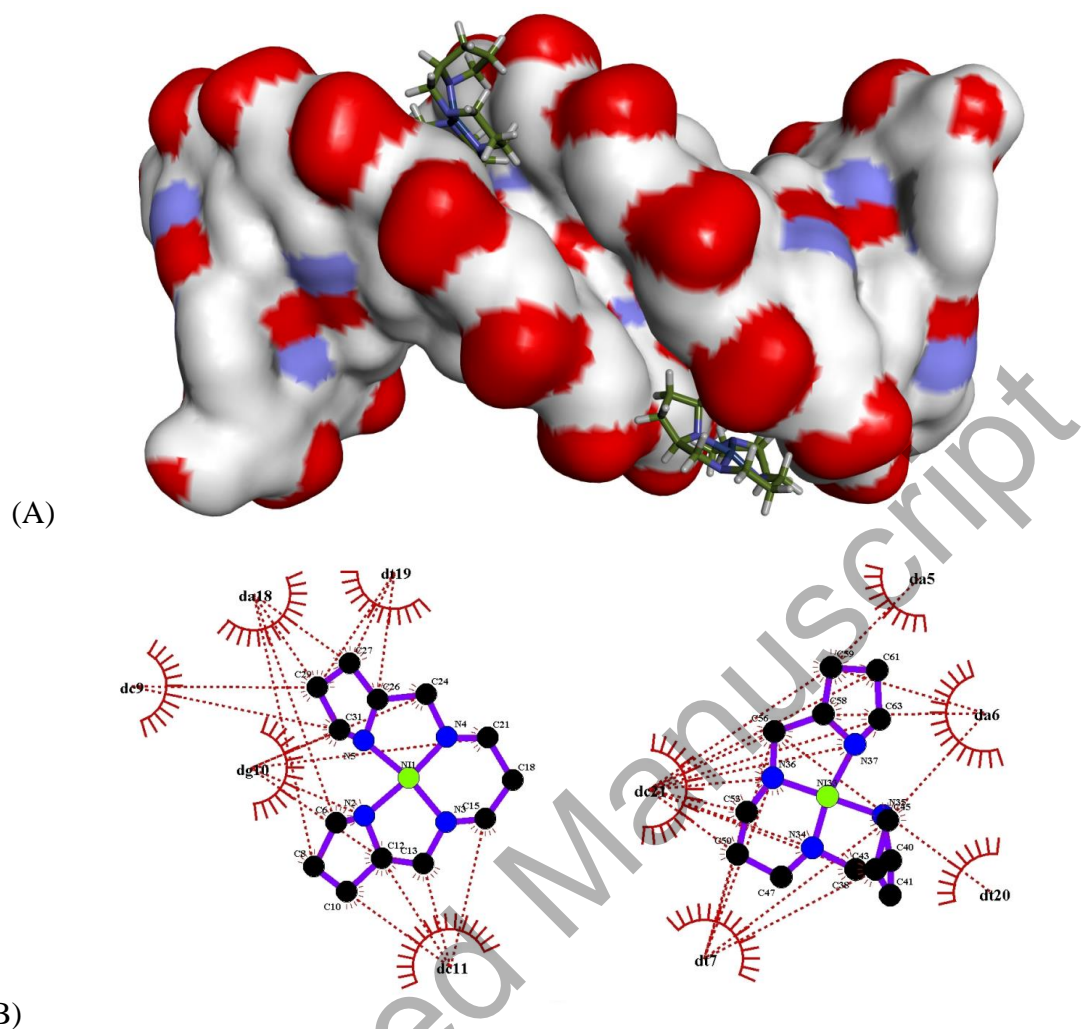


Figure 6. (A) Molecular docked model of complex **1** with duplex DNA dodecamer (PDB ID:1BNA). The full view of docking between nickel complex and 1BNA with molecular surface. (B) The binding mode between ligand and duplex DNA; red-dashed lines indicate hydrophobic interactions between them. The ligand molecule is represented as stick.

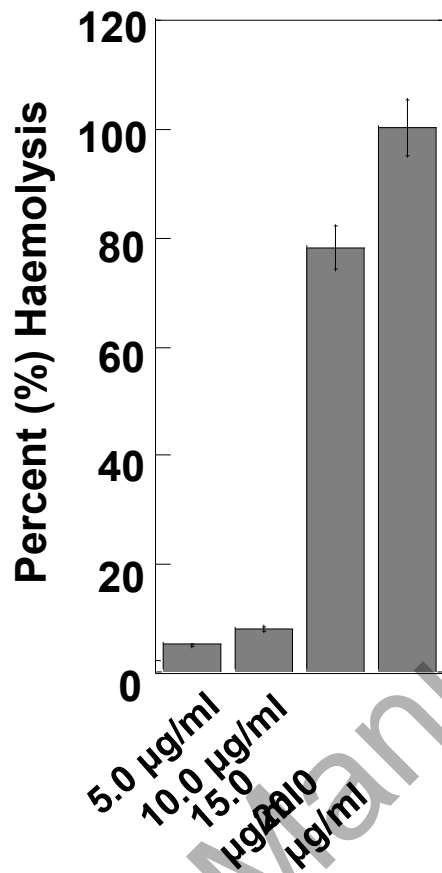


Figure 7. Percentage PBMC viability measured by Trypan Blue exclusion method.

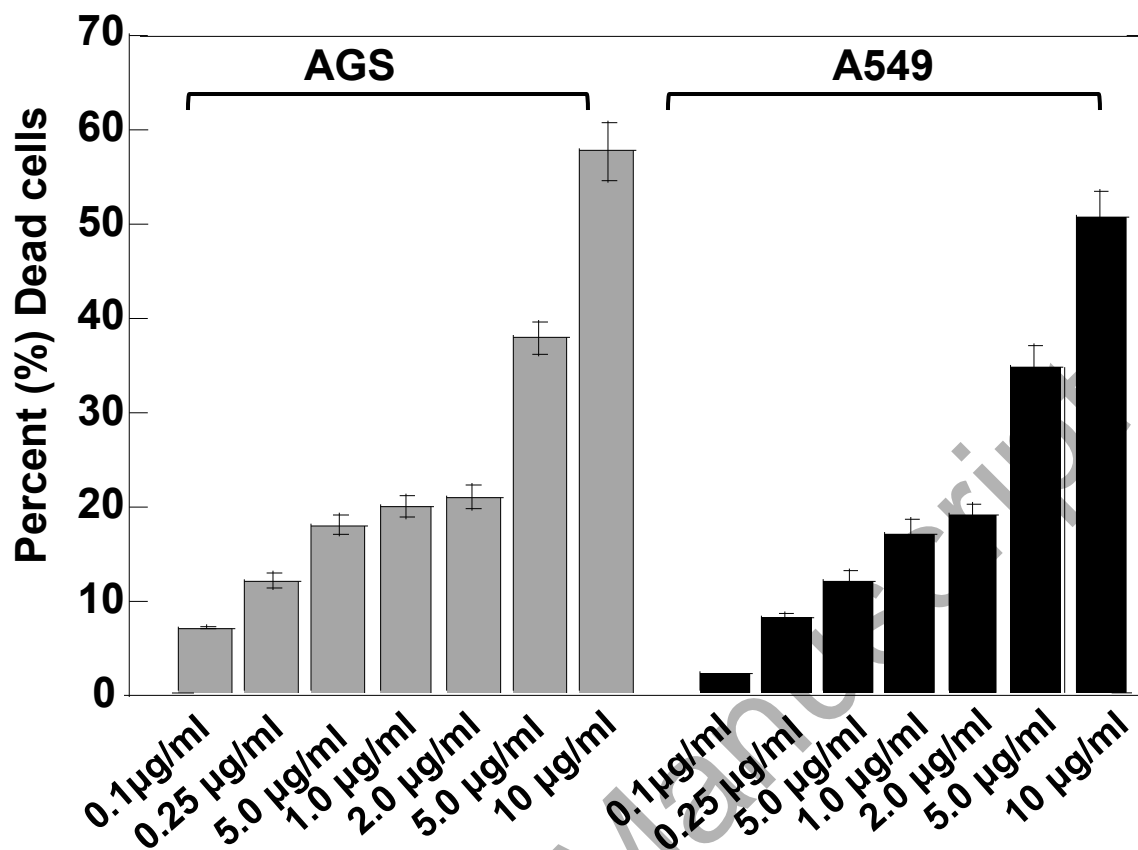


Figure 8. A549 and AGS cell viability measured by MTT assay at various concentrations of complex 1.

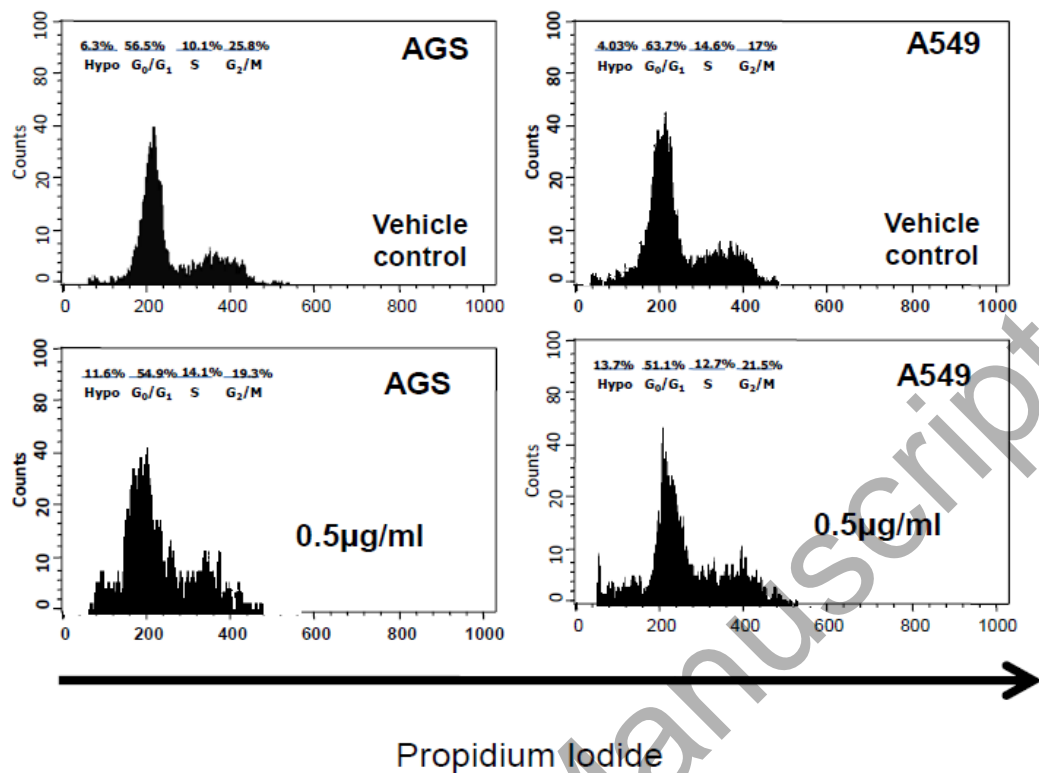


Figure 9. Cell cycle analysis of treated and untreated AGS and A549 cells by flow cytometer using propidium iodide (PI) as DNA-binding fluorochrome. Histogram display of DNA content (x-axis, PI-fluorescence) versus counts (y-axis) has been shown. The upper and lower panels display cell cycle phase distribution of treated and untreated AGS cells with wild type p53 and silenced p53, respectively.

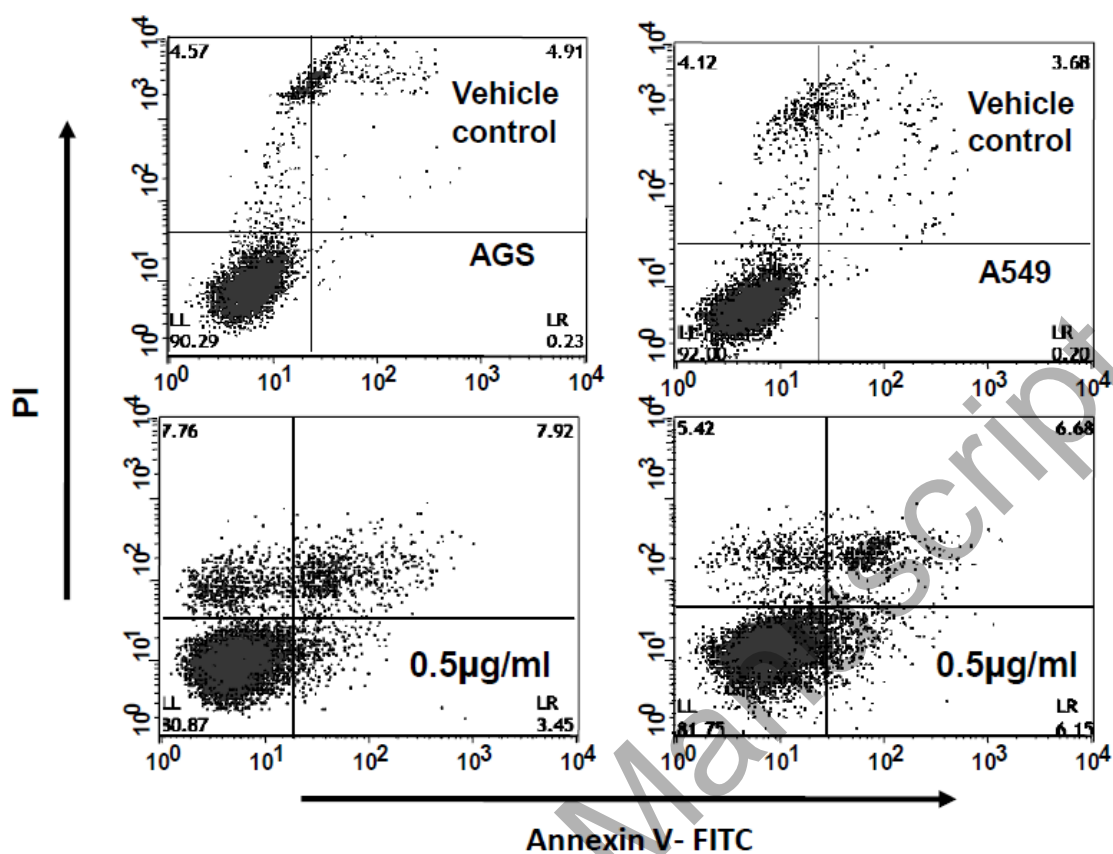


Figure 10. Annexin V assay in AGS and A549 cells. Dual parameter dot plot of FITC-fluorescence (x-axis) versus PI-fluorescence (y-axis) has been shown in logarithmic fluorescence intensity. Quadrants: lower left, live cells; lower right, apoptotic cells; upper right, necrotic cells. The upper and lower panels demonstrated apoptosis induction in treated and untreated AGS cells with wild type p53 and silenced p53, respectively.

Table 1. Crystal data and details of the structure determination for complex **1**.

Formula	C <sub>13</sub> H <sub>14</sub> N <sub>4</sub> Ni
Formula weight	284.97
Crystal system	Monoclinic
Space group	P21/n (No. 14)
a, b, c [Å]	9.9893(2), 9.1834(2), 26.8760(5)
alpha, beta, gamma [°]	90, 99.566(2), 90
V [Å <sup>3</sup> ]	2431.21(9)
Z	8
D <sub>(calc)</sub> [g/cm <sup>3</sup> ]	1.557
μ (MoKα) [mm]	1.582
F(000)	1184
Crystal size [mm]	0.24 × 0.25 × 0.36
Temperature [K]	100
Radiation [Å]	MoKα, 0.71073
Theta min-max [°]	3.0, 27.0
Dataset	-11:12; -11:10; -33:34
Tot., Uniq. data, R(int)	11714, 5241, 0.029
Observed data [I > 2.0 σ(I)]	4492
Nref, Npar	5241, 325
R, wR2, S	0.0328, 0.0763, 1.06
Min. and max. resd. dens. [e/Å <sup>3</sup> ]	-0.42, 0.44



Table 2. Selected bond lengths (Å) and angles (°) for complex **1**.

Bond lengths (Å)		Bond lengths (Å)	
Ni1-N1	1.8953(19)	Ni2-N7	1.8951(19)
Ni1-N2	1.9086(19)	Ni2-N5	1.9119(19)
Ni1-N3	1.8993(19)	Ni2-N6	1.8930(19)
Ni1-N4	1.8854(19)	Ni2-N8	1.9002(19)
Bond angles (°)		Bond angles (°)	
N1-Ni1-N2	84.17(8)	N6-Ni2-N7	176.92(8)
N1-Ni1-N3	173.14(8)	N6-Ni2-N8	98.67(8)
N1-Ni1-N4	98.34(8)	N7-Ni2-N8	84.05(8)
N2-Ni1-N3	94.01(8)	N5-Ni2-N8	176.65(8)
N2-Ni1-N4	175.94(8)	N5-Ni2-N6	83.94(8)
N3-Ni1-N4	83.87(8)	N5-Ni2-N7	93.40(8)

Accepted Manuscript

Table 3. Stern-Volmer quenching constant ( $K_{sv}$ ), quenching rate constant ( $K_q$ ), binding constant ( $K_b$ ), apparent binding constant ( $K_{app}$ ) and number of binding sites ( $n$ ) for the interaction of complex **1** with CT-DNA solution.

	<b>1</b>
$K_{sv} (M^{-1})$	$3.534(\pm 0.078) \times 10^4$
$K_q (M^{-1})$	$3.534(\pm 0.078) \times 10^{12}$
$K_b (M^{-1})$	$7.582(\pm 0.016) \times 10^3$
$K_{app} (M^{-1})$	$2.86 \times 10^4$
$n$	$1.09079 \pm 0.1488$

Table 4. Stern-Volmer quenching constant ( $K_{sv}$ ), quenching rate constant ( $K_q$ ), binding constant ( $K_b$ ) and number of binding sites ( $n$ ) for the interaction of complex **1** with BSA and HSA.

	<b>BSA</b>	<b>HSA</b>
$K_{sv} (M^{-1})$	$4.83(\pm 0.034) \times 10^4$	$3.59(\pm 0.066) \times 10^4$
$K_q (M^{-1})$	$4.83(\pm 0.034) \times 10^{12}$	$3.59(\pm 0.066) \times 10^{12}$
$K_b (M^{-1})$	$1.80(\pm 0.317) \times 10^5$	$0.741(\pm 0.088) \times 10^5$
$n$	$1.15891 \pm 0.0691$	$1.07374 \pm 0.0193$

Table 5. Interaction energy (in kcal/mol) between complex **1** and B-DNA.

Energy	<b>1</b>
Interaction energy	-1,046.8
van der Waals interaction	-42.3422
Electrostatic interaction	-1,004.46

Table 6. Representative examples of metal complexes along with complex **1** for cytotoxicity studies on two different cell lines (AGS and A549).

Complex	IC <sub>50</sub> (μM)		References
	AGS	A549	
[Ni(L)] (C <sub>13</sub> H <sub>14</sub> N <sub>4</sub> Ni)	15.09	35.09	Current paper
<i>Cis-platin</i>		25±0.46	[104]
Ni(L) <sub>2</sub> (C <sub>34</sub> H <sub>28</sub> N <sub>4</sub> NiO <sub>2</sub> S <sub>2</sub> )		14.06	[95]
[NiL <sub>2</sub> (phen)]·3CH <sub>3</sub> OH		39.5±1.0	[96]
Bis((Z)-N-methyl-2-(2-oxoindolin-3-ylidene)thiosemicarbazonato)nickel(II), (C <sub>20</sub> H <sub>18</sub> N <sub>8</sub> NiO <sub>2</sub> S <sub>2</sub> )		18.4	[103]
Bis((Z)-2-(1-allyl-2-oxoindolin-3-ylidene)thiosemicarbazonato)nickel(II), (C <sub>26</sub> H <sub>26</sub> N <sub>8</sub> NiO <sub>2</sub> S <sub>2</sub> )		< 0.1	[103]
Bis((Z)-N-methyl-2-(1-methyl-2-oxoindolin-3-ylidene)-thiosemicarbazonato)nickel(II), (C <sub>22</sub> H <sub>22</sub> N <sub>8</sub> NiO <sub>2</sub> S <sub>2</sub> )		5.7	[103]
Bis((Z)-2-(1-benzyl-2-oxoindolin-3-ylidene)thiosemicarbazonato)nickel(II), (C <sub>34</sub> H <sub>30</sub> N <sub>8</sub> NiO <sub>2</sub> S <sub>2</sub> )		11.5	[103]
Bis((Z)-2-(5-bromo-1-methyl-2-oxoindolin-3-ylidene)-thiosemicarbazonato)nickel(II), (C <sub>20</sub> H <sub>16</sub> Br <sub>2</sub> N <sub>8</sub> NiO <sub>2</sub> S <sub>2</sub> )		29.3	[103]
[NiL <sub>2</sub> (phen)]·CH <sub>3</sub> CN		29.19±1.10	[106]
[Ni(1-(anthracen-9-yl)-N-(1H-benzo[d]imidazole-2-yl)methanimine)Cl <sub>2</sub> ], (C <sub>22</sub> H <sub>15</sub> N <sub>3</sub> NiCl <sub>2</sub> )	23.6±0.7		[107]
[Ni(1-(anthracen-9-yl)-N(benzo[d]thiazol-2-yl)methanimine)Cl <sub>2</sub> ], (C <sub>22</sub> H <sub>14</sub> N <sub>2</sub> SNiCl <sub>2</sub> )	10.8±0.6		[107]
[Ni <sub>2</sub> (H <sub>2</sub> L <sup>1</sup> ) <sub>2</sub> (OAc) <sub>2</sub> (C <sub>2</sub> H <sub>5</sub> OH) <sub>2</sub> ] <sub>2</sub> , (C <sub>32</sub> H <sub>50</sub> N <sub>2</sub> Ni <sub>2</sub> O <sub>12</sub> )		>50	[8]
Ni <sub>2</sub> (S-L <sup>1</sup> ) <sub>2</sub> (OC <sub>2</sub> H <sub>5</sub> ) <sub>2</sub> (OCOCH <sub>3</sub> ) <sub>2</sub> , (C <sub>42</sub> H <sub>50</sub> N <sub>2</sub> Ni <sub>2</sub> O <sub>12</sub> )		59.01±1.77	[97]
Ni <sub>2</sub> (R-L <sup>1</sup> ) <sub>2</sub> (OC <sub>2</sub> H <sub>5</sub> ) <sub>2</sub> (OCOCH <sub>3</sub> ) <sub>2</sub> , (C <sub>42</sub> H <sub>50</sub> N <sub>2</sub> Ni <sub>2</sub> O <sub>12</sub> )		43.72±1.64	[97]
[Ni <sub>2</sub> (Msal-tsc) <sub>2</sub> (μ-dppm)]		26	[102]
[Ni <sub>2</sub> (Msal-mtsc) <sub>2</sub> (μ-dppm)]		23	[102]
[Ni <sub>2</sub> (Msaletsc) <sub>2</sub> (μ-dppm)]		12	[102]
[Ni <sub>2</sub> (Msal-ptsc) <sub>2</sub> (μ-dppm)]		20	[102]
[Ni <sub>4</sub> (HL <sup>2</sup> ) <sub>3</sub> (μ <sub>3</sub> -O)(H <sub>2</sub> O) <sub>3</sub> ]·9H <sub>2</sub> O, (C <sub>39</sub> H <sub>84</sub> N <sub>3</sub> Ni <sub>4</sub> O <sub>31</sub> )		>50	[8]
[Cu(H <sub>2</sub> L <sup>1</sup> )Cl]·CH <sub>3</sub> OH, (C <sub>13</sub> H <sub>20</sub> ClCuNO <sub>4</sub> )		>50	[8]
2-(1-Allyl-2-oxoindolin-3-ylidene)-N-cyclohexylhydrazinecarbothioamide copper(II), (C <sub>18</sub> H <sub>21</sub> ClCuN <sub>4</sub> OS)		88.59	[66]
2-(2-Oxo-1-(prop-2-yn-1-yl)indolin-3-ylidene)-N-cyclohexylhydrazinecarbothioamide copper(II), (C <sub>18</sub> H <sub>19</sub> ClCuN <sub>4</sub> OS)		99.53	[66]
[Cu(L)(ClO <sub>4</sub> )], (C <sub>19</sub> H <sub>13</sub> Cl <sub>2</sub> CuNO <sub>5</sub> S)		21.06	[105]
[Cu(L)(phen)](ClO <sub>4</sub> ), (C <sub>31</sub> H <sub>21</sub> Cl <sub>2</sub> CuN <sub>3</sub> O <sub>5</sub> S)		15.93	[105]
[Cu(L)(bpy)](ClO <sub>4</sub> ), (C <sub>29</sub> H <sub>21</sub> Cl <sub>2</sub> CuN <sub>3</sub> O <sub>5</sub> S)		12.32	[105]
[Cu(L)(dmbpy)](ClO <sub>4</sub> ), (C <sub>31</sub> H <sub>25</sub> Cl <sub>2</sub> CuN <sub>3</sub> O <sub>5</sub> S)		18.74	[105]
[Cu(1-(anthracen-9-yl)-N-(1H-benzo[d]imidazole-2-yl)methanimine)Cl <sub>2</sub> ],	10.2±0.4		[107]

(C <sub>22</sub> H <sub>15</sub> N <sub>3</sub> CuCl <sub>2</sub> )			
[Cu(1-(anthracen-9-yl)-N(benzo[d]thiazol-2-yl)methanimine)Cl <sub>2</sub> ], (C <sub>22</sub> H <sub>14</sub> N <sub>2</sub> SCuCl <sub>2</sub> )	8.9±0.6		[107]
[Cu(L)(phen)](ClO <sub>4</sub> ), (C <sub>23</sub> H <sub>18</sub> CuN <sub>7</sub> S)	8.9±0.3		[98]
[Cu(L)(bpy)](ClO <sub>4</sub> ), (C <sub>21</sub> H <sub>18</sub> CuN <sub>7</sub> S)	10.8±0.5		[98]
[Cu(L)(dmbpy)](ClO <sub>4</sub> ), (C <sub>23</sub> H <sub>22</sub> CuN <sub>7</sub> S)	9.4±0.4		[98]
[Cu(L)(dpa)](ClO <sub>4</sub> ), (C <sub>21</sub> H <sub>19</sub> CuN <sub>8</sub> S)	25.2±0.6		[98]
2-(1-Benzyl-2-oxoindolin-3-ylidene)-Ncyclohexylhydrazinecarbo- thioamide copper(II), (C <sub>44</sub> H <sub>46</sub> C <sub>12</sub> Cu <sub>2</sub> N <sub>8</sub> O <sub>2</sub> S <sub>2</sub> )		82.56	[66]
[Cu(L) <sub>2</sub> (N <sub>3</sub> ) <sub>2</sub> ], (C <sub>16</sub> H <sub>18</sub> Cu <sub>2</sub> N <sub>14</sub> S <sub>2</sub> )	4.3	10	[99]
[Cu <sub>4</sub> (HL <sup>2</sup> ) <sub>2</sub> (H <sub>2</sub> L <sup>2</sup> ) <sub>2</sub> (H <sub>2</sub> O)(C <sub>2</sub> H <sub>5</sub> OH)]·(ClO <sub>4</sub> ) <sub>2</sub> ·2(C <sub>2</sub> H <sub>5</sub> OH), (C <sub>58</sub> H <sub>88</sub> Cu <sub>4</sub> Cl <sub>2</sub> N <sub>4</sub> O <sub>28</sub> )		16.05	[8]
[CoL <sub>2</sub> (phen)]·3CH <sub>3</sub> OH, (C <sub>53</sub> H <sub>50</sub> N <sub>6</sub> O <sub>5</sub> Co)		58.9±1.2	[96]
[CoL <sub>2</sub> (phen)]·CH <sub>3</sub> CN·HL, (C <sub>52</sub> H <sub>41</sub> N <sub>7</sub> O <sub>4</sub> Co)		33.40±2.45	[106]
[Ru(H-Nap-tsc)(CO)Cl(PPh <sub>3</sub> ) <sub>2</sub> ]		20±0.19	[100]
[Ru(Nap-tsc)(CO)(PPh <sub>3</sub> ) <sub>2</sub> ]		17±0.13	[100]
[RuNi(Nap-tsc)(CO)Cl(PPh <sub>3</sub> ) <sub>3</sub> ]		18±0.15	[100]
[Ru(H-Sal-etsc)(CO)Cl(PPh <sub>3</sub> ) <sub>2</sub> ]		20±1.10	[101]
[Ru(Sal-etsc)(CO)(PPh <sub>3</sub> ) <sub>2</sub> ].Cl		17±0.93	[101]
[Ru(H-Sal-mtsc)(CO)Cl(PPh <sub>3</sub> ) <sub>2</sub> ]		20±0.51	[104]
[Ru(Sal-mtsc)(CO)(PPh <sub>3</sub> ) <sub>2</sub> ]		15±0.97	[104]
[RuNi(Nap-tsc)(CO)Cl(PPh <sub>3</sub> ) <sub>3</sub> ]		18±0.15	[100]